scientific reports

OPEN

An intelligent framework for skin cancer detection and classification using fusion of Squeeze-Excitation-DenseNet with Metaheuristic-driven ensemble deep learning models

J. D. Dorathi Jayaseeli[1], J Briskilal[2], C. Fancy[3], V. Vaitheeshwaran[4], R. S. M. Lakshmi Patibandla[5], Khasim Syed[6]✉ & Anil Kumar Swain[7]

Skin cancer is the most dominant and critical method of cancer, which arises all over the world. Its damaging effects can range from disfigurement to major medical expenditures and even death if not analyzed and preserved timely. Conventional models of skin cancer recognition require a complete physical examination by a specialist, which is time-wasting in a few cases. Computer-aided medicinal analytical methods have gained massive popularity due to their efficiency and effectiveness. This model can assist dermatologists in the initial recognition of skin cancer, which is significant for early diagnosis. An automatic classification model utilizing deep learning (DL) can help doctors perceive the kind of skin lesion and improve the patient's health. The classification of skin cancer is one of the hot topics in the research field, along with the development of DL structure. This manuscript designs and develops a Detection of Skin Cancer Using an Ensemble Deep Learning Model and Gray Wolf Optimization (DSC-EDLMGWO) method. The proposed DSC-EDLMGWO model relies on the recognition and classification of skin cancer in biomedical imaging. The presented DSC-EDLMGWO model initially involves the image preprocessing stage at two levels: contract enhancement using the CLAHE method and noise removal using the wiener filter (WF) model. Furthermore, the proposed DSC-EDLMGWO model utilizes the SE-DenseNet method, which is the fusion of the squeeze-and-excitation (SE) module and DenseNet to extract features. For the classification process, the ensemble of DL models, namely the long short-term memory (LSTM) technique, extreme learning machine (ELM) model, and stacked sparse denoising autoencoder (SSDA) method, is employed. Finally, the gray wolf optimization (GWO) method optimally adjusts the ensemble DL models' hyperparameter values, resulting in more excellent classification performance. The effectiveness of the DSC-EDLMGWO approach is evaluated using a benchmark image database, with outcomes measured across various performance metrics. The experimental validation of the DSC-EDLMGWO approach portrayed a superior accuracy value of 98.38% and 98.17% under HAM10000 and ISIC datasets across other techniques.

Keywords Skin Cancer detection, Ensemble deep learning, Gray Wolf optimization, Feature extraction, Image preprocessing

[1]Department of Computing Technologies, SRM Institute of Science and Technology, Kattankulathur 603203, India. [2]Department of Computing Technologies, Faculty of Engineering and Technology, SRM Institute of Science and Technology, Kattankulathur 603203, Chennai, India. [3]Department of Networking and Communications, SRM Institute of Science and Technology, Kattankulathur 603203, Chennai, India. [4]Department of Computer Science and Engineering, Aditya University, Surampalem, Kakinada, India. [5]Department of Computer Science and Engineering, Koneru Lakshmaiah Education Foundation, Vaddeswaram, Guntur, Andhra Pradesh, India. [6]School of Computer Science & Engineering, VIT - AP University, Amaravati 522237, Andhra Pradesh, India. [7]KIIT Deemed to be University, Bhubaneswar 751024, Odisha, India. ✉email: profkhasim@gmail.com

Skin cancer is the most predominant cancer type and starts with the uncontrolled reproduction of skin cells. It may arise owing to the ultraviolet radiation from tanning beds or sunshine, forming malignant tumours, and its reason for increasing skin cells[1]. There are two major kinds of skin cancer such as melanoma and non-melanoma. A dissimilar sort of skin cancer is melanoma; this type can cause a 75% death rate[2]. The death rate of melanoma existence is predicted to increase in the future decades. The critical stage for treating skin cancer is accurate and primary recognition[3]. For instance, if melanoma is not analyzed early, it increases and spreads around the exterior skin layer. Specifically, why it is essential to examine it in the primary phase when the death rate decreases and effective treatment is possible[4]. The most common approach to analyzing skin cancer is visual investigations by professionals, which have a precision of nearly 60%. Among many kinds, dermoscopy images are attained by specialized instruments, leading to higher-resolution skin imaging with a reduction of the skin surface reflectance[5]. Dermoscopy raises the melanoma analysis precisely, but it can still be difficult to analyze some lesions, mainly initial melanomas, precisely and the absence of unique dermoscopic features. Multiple approaches were designed for the automatic detection of melanoma-affected skin portions. Initially, handcrafted features-related approaches were introduced for analyzing melanoma[6].

However, such approaches did not generate better results due to divergences in the melanoma moles' size, colour, and shape. Various computer-aided diagnosis (CAD) methods have recently been presented for skin cancer detection. These methods generally depend on classical computer vision (CV) models to extract several features to sustain a classifier[7]. DL and machine learning (ML) approaches have recently become trends in dealing with this challenge. Amongst these diverse CAD, DL-based approaches give favourable outcomes in classifying and segmenting skin lesions owing to their capability to remove composite features from skin lesion images with more elaboration[8]. DL structures to remove many features utilizing Convolutional Neural Networks (CNNs). CNN can excerpt features effectively related to classical approaches for feature extraction. DL-based computer-assisted methods have recently been employed to analyze diverse diseases and have shown greater outcomes. Among these, DL approaches, specifically CNNs, have illustrated superior performance in classifying and segmenting skin lesions due to their capability to automatically learn complex patterns from large image datasets[9]. Unlike conventional methods, CNNs can capture hierarchical features, which enable them to adapt and generalize better to discrepancies in skin lesion images. Recent improvements have shown that DL-based systems not only enhance diagnostic accuracy but also mitigate the dependency on manual intervention, allowing for faster and more reliable disease detection. The integration of these models with improved optimization techniques additionally elevates their potential, resulting in more robust and precise results in skin cancer diagnosis[10].

This manuscript designs and develops a Detection of Skin Cancer Using an Ensemble Deep Learning Model and Gray Wolf Optimization (DSC-EDLMGWO) method. The proposed DSC-EDLMGWO model relies on the recognition and classification of skin cancer in biomedical imaging. The presented DSC-EDLMGWO model initially involves the image preprocessing stage at two levels: contract enhancement using the CLAHE method and noise removal using the wiener filter (WF) model. Furthermore, the proposed DSC-EDLMGWO model utilizes the SE-DenseNet method, which is the fusion of the squeeze-and-excitation (SE) module and DenseNet to extract features. For the classification process, the ensemble of DL models, namely the long short-term memory (LSTM) technique, extreme learning machine (ELM) model, and stacked sparse denoising autoencoder (SSDA) method, is employed. Finally, the gray wolf optimization (GWO) method optimally adjusts the ensemble DL models' hyperparameter values, resulting in greater classification performance. The effectiveness of the DSC-EDLMGWO approach is evaluated using a benchmark image database, with outcomes measured across various performance metrics. The key contribution of the DSC-EDLMGWO approach is listed below.

- The DSC-EDLMGWO method utilizes CLAHE and WF-based preprocessing to improve image quality by mitigating noise and improving contrast. This preprocessing step confirms that the input images are optimized for enhanced feature extraction and classification. By improving image clarity, the model improves the accuracy of subsequent stages, resulting in more reliable results.
- The DSC-EDLMGWO model employed the SE-DenseNet approach for effective feature extraction, enabling it to capture and highlight the most relevant features from input images. This approach improves the technique's capability to identify complex patterns and structures in the data. By integrating SE-DenseNet, the model improves its overall performance in recognizing and classifying skin lesions.
- The classification step incorporates an ensemble of DL techniques, comprising LSTM, ELM, and SSDA, to improve prediction accuracy and robustness. This incorporation utilizes the merits of each model, improving the approach's capability to handle diverse data. An ensemble approach makes the model more reliable in accurately classifying skin lesions.
- The DSC-EDLMGWO methodology implemented the GWO model to fine-tune the model parameters, optimizing the search for the best solution. This improves the technique's overall performance by refining the weights and improving its generalization ability. By using GWO, the model is better equipped to handle unseen data and provide more accurate results.
- The novelty of the DSC-EDLMGWO model is in its unique integration of advanced preprocessing techniques, comprising CLAHE and WF, with a hybrid ensemble of DL methods, namely LSTM, ELM, and SSDA. Furthermore, the utilization of the GWO method for fine-tuning model parameters significantly improves both accuracy and efficiency. This approach provides a more robust and efficient solution for skin cancer detection, setting it apart from conventional methods.

Literature of works

Farea et al.[11] presented a new solution for a hybrid AI platform for skin cancer forecasting. This structure contains two pivotal stages: Initially, an inclusive skin cancer database is organized by associating different public databases that include several diseases. DL optimization is precisely performed through the Artificial Bee Colony (ABC) approach, efficiently mitigating the possible harmful effect of primary parameter randomness on AI method performance. Keerthana et al.[12] introduce two innovative hybrid CNN methods at an output layer for categorizing images. These features are removed from both CNN methods, combined, and provided for classification. This label was acquired from professional dermatologists and utilized as a reference to calculate the developed method's performance. Saleh et al.[13] focused on several advanced techniques for skin cancer classification. CNN is a kind of Inception V3; AlexNet, ResNet 50, and MobileNet V2 were applied as feature extractors. Feature extraction was implemented using dual grey wolf optimizer (GWO) models and novel features. Skin cancer imageries were categorized into four groups depending on six ML classifiers. Albawi et al.[14] project and apply an NN-based model for skin cancer forecasting to show the strength of NN in this area. This approach evaluates the DL types that are best for analyzing diseases that precisely overtake human capability for accuracy and speed and evaluates the optimal number of neurons and layers to attain the finest possible accuracy. In[15], a SkinMultiNet structure that depends on TL principles was developed. The presented method incorporates the Xception and InceptionV3 CNN methods for forecasting skin cancer by applying image data. Whereas other ML methods like NasNet, MobileNet, and ResNet50 were discovered, the SkinMultiNet structure shows positive outcomes. In[16], fuzzy logic-based image segmentation and a modified DL method were projected. This dermoscopic image development was attained by utilizing preprocessing methods, the L-R fuzzy defuzzification, standard deviation, and infusion of mathematical logical approaches to improve the segmentation outcomes. Musthafa et al.[17] projected an advanced CNN method designed for the nuanced challenge of skin lesion identification. This method structure was intricately intended with many pooling, dense layers, and convolutional focused on capturing the complex visual characteristics of skin lesions. This research develops a CNN method with data augmentation and optimized layer configuration, extensively boosting analytical accuracy in skin cancer detection. The authors[18] offer an automatic image-based approach for categorizing and diagnosing skin problems that utilize ML classification. Computational models are used to relegate, analyze, and process picture data. Skin photographs are initial filters to extract unwanted noise from images and then processed to improve the overall picture quality. Features are removed from an image by employing sophisticated models like CNN and classifying the image by applying the softmax model. Huang et al.[19] propose the self-paced learning absolute network-based logistic regression (SLNL) model by incorporating self-paced learning with absolute network-based logistic regression to enhance gene selection and interpretability and mitigate noise impact, resulting in improved prediction accuracy.

Ozdemir and Pacal[20] present a lightweight hybrid model by integrating ConvNeXtV2 and focal self-attention to tackle data imbalance and model complexity, improving feature extraction and focusing on key regions for enhanced sensitivity. Wang et al.[21] introduce the Merge-and-Split Graph Convolution module for extracting rich semantic information, a Short-term Dependence module for joint and motion features, and the Hierarchical Guided Attention Module (HGAM) method to emphasize relevant hierarchical interaction information. Pascal[22] evaluated DL methods for cervical cancer diagnosis. Cui, Ding, and Chen[23] propose a hybrid-directed hypergraph convolution network (H-DHGCN) to model high-order human skeleton relationships. It integrates a static-directed hypergraph for joint relations and a dynamic-directed hypergraph (D-DHG) that adapts to motion sequence characteristics. Bayram et al.[24] explore the role of the DL technique in diagnosing cerebral vascular occlusions. Pacal, Alaftekin, and Zengul[25] improve the Swin Transformer by replacing shifted window-based multi-head self-attention (SW-MSA) with hybrid shifted window-based multi-head self-attention (HSW-MSA) for better skin cancer overlap processing and utilizing a SwiGLU-based MLP for improved accuracy and training efficiency. Khan et al.[26] propose a novel manta-ray foraging optimizer (MRFO)-based method integrated with enhanced residual blocks in DenseNet-169 to optimize tumour feature representation. By fine-tuning hyperparameters with MRFO and integrating enhanced residual blocks, the model's performance is significantly improved for tumour detection. Bing et al.[27] propose an efficient ECG denoising strategy integrating S-transform, bi-dimensional empirical mode decomposition, and non-local means to remove noise while preserving signal characteristics. Khan, Alam, and Ahmed[28] present an automated CAD system for multiclass skin cancer classification. It fine-tunes models across seven cancer classes and compares the performance of three pre-trained CNNs and three ensemble models to improve classification accuracy. Song et al.[29] present a cluster centre transformer for dental plaque segmentation that groups pixels based on intensity and texture, enhancing accuracy by concentrating on local contours and edges. A pyramid fusion mechanism improves low-contrast features for better segmentation. Das and Mohanty[30] introduce a homogeneous ensemble learning technique, EnsembleSVM, for skin cancer detection. It comprises two parallel SVM models trained with balanced and augmented data, respectively, followed by a final SVM model for classification. Jia, Chen, and Chi[31] utilize a pre-trained U-Net for retinal vessel segmentation and integrate the result into the generator with a spatial feature transform layer. Channel and spatial attention modules improve the discriminator, while the L1 loss function enhances super-resolution image accuracy by comparing segmentation map differences. Ozdemir and Pacal[32] introduce a hybrid DL methodology by incorporating ConvNeXtV2 blocks and separable self-attention to improve feature extraction and classification. This model captures fine-grained local features, while separable self-attention prioritizes relevant regions with reduced computational cost.

Bilal et al.[33] integrate an improved quantum-inspired binary Grey Wolf Optimizer (GWO) with a Support Vector Machine (SVM) for improved breast cancer classification. Sainudeen and Sathyalakshmi[34] present a six-phase skin cancer classification model, utilizing an improved deep joint segmentation (IDJS) for segmentation and CLAHE for contrast enhancement. Features are extracted with Gray Level Co-occurrence Matrix (GLCM), Color Coherence Vector (CCF), Local Gradient Intensity Pattern (LGIP), and Median Ternary Pattern (MTP), followed by data augmentation. Finally, an ensemble classification is performed with deep maxout, LSTM, and CNN models. Bilal et al.[35] introduce a hybrid model integrating an Extreme Learning Machine (ELM) with FuNet transfer learning (TL) and an Enhanced Quantum-Genetic Binary Grey Wolf Optimizer (Q-GBGWO) methodology, optimizing feature extraction for improved breast cancer classification. Akter et al.[36] present a hybrid DL framework for skin cancer classification, employing pre-trained models InceptionV3 and DenseNet121. The model improves accuracy through data preprocessing and combines predictions utilizing a weighted sum rule for enhanced generalization. Bilal et al.[37] present NIMEQ-SACNet, a hybrid model incorporating Enhanced Quantum-Inspired Binary Grey Wolf Optimizer (EQI-BGWO) with a self-attention capsule network, improving VTDR classification accuracy through optimized parameter calibration. Vidhyalakshmi and Kanchana[38] employ deep neural network (DNN) and Keras DNN (KDNN) classifiers to identify skin cancer stages, with preprocessing to simplify classification. Features are selected, and segmentation is performed utilizing GrabCut and CSO methods. Wu et al.[39] aim to explore the clinical characteristics, outcomes, and treatment of subacute cutaneous lupus erythematosus (SCLE) induced by PD-1/PD-L1 inhibitors. Chiu et al.[40] developed an AI diagnostic model using TL with eight pre-trained models to classify skin cancer into three categories. The two-stage classification enhances accuracy and mitigates false negatives. Pascal[41] proposes an advanced DL approach utilizing the Swin Transformer with a Hybrid Shifted Windows Multi-Head Self-Attention (HSW-MSA) module and a rescaled model, improving classification accuracy, reducing memory usage, and improving training speed with a Residual-based MLP (ResMLP). Reis and Turk[42] introduce two early skin cancer detection methods using AI. The first method introduces DSCIMABNet, integrating multi-head attention and depthwise separable convolution for flexible feature learning. The second method improves classification performance by incorporating DSCIMABNet with ensemble learning and models trained on ImageNet. Hosseinzadeh et al.[43] assist healthcare experts in distinguishing between benign and malignant skin cancer utilizing ML and DL models. It utilizes TL approaches such as DenseNet-201 for feature extraction and a feature selection layer with methods like Lasso, Principal Component Analysis (PCA), and Random Forest (RF) to improve evaluation metrics.

The reviewed studies highlight significant advancements in AI and DL methods for skin cancer detection, yet various limitations and research gaps remain. Many methods depend heavily on large, high-quality datasets, which may not be universally available and may not apply to diverse patient populations. Moreover, while integrating multiple models (e.g., CNN, SVM, and ensemble methods) has exhibited promise, model interpretability remains a key challenge, specifically for clinical adoption. Many models also face difficulty with data imbalance and fail to generalize well across diverse datasets. Further, the concentration on enhancing classification accuracy has often overlooked the practical deployment of these models in real-time, needing consideration of computational efficiency and resource constraints. Additionally, improvements in model explainability and robust evaluation metrics are necessary for translating AI-based diagnostic tools into mainstream healthcare settings.

Materials and methods

This manuscript presents a DSC-EDLMGWO method. The proposed DSC-EDLMGWO model relies upon skin cancer detection in biomedical imaging. It accomplishes this through various stages, such as image preprocessing, feature extraction, classification, and a hyperparameter tuning process. Figure 1 epitomizes the overall workflow of the DSC-EDLMGWO model.

Image preprocessing

The DSC-EDLMGWO method first applies image preprocessing, which involves dual stages such as contrast enhancement using CLAHE and noise removal using the WF.

Contrast enhancement using CLAHE

CLAHE is a novel example of the HE model, which works adaptably on the image being improved. It is the model applied to enhance the local contrast of the images[44]. It is an improved form of AHE, neither of which overwhelms the restrictions of regular HE. It constitutes the generality of AHE and standard HE, while the histograms are computed for the contextual area of the pixel. These pixel intensities are, therefore, converted to the value inside the display area consistent with the intensities of the pixel grade within the local histogram intensities. It has been initially established for diagnostic images and has been demonstrated to be effective for developing lower-contrast images like segmented films. Bilinear interpolation has been applied to prevent visibility on the area border. The main difficulty using CLAHE models is that they frequently improve the image by making them named contrast objects hidden in the unique images. The enhanced image often doesn't look natural and is disturbing.

Noise removal using WF

To enhance image clarity and reduce noise and blurriness in the image, a WF is applied. The WF is a robust linear noise elimination model that successfully decreases the influence of white noise in images[45]. First, colour images are split into individual colour channels, and each channel is processed independently during the noise elimination phase. The Fourier Transform (FT) is applied to each colour channel separately to enhance the filter's efficiency, converting the image from the spatial domain to the frequency domain. After filtering each channel independently, the channels are combined to reconstruct the filtered colour image in the spatial domain. The WF is applied throughout this process to effectively handle noise while preserving the integrity of the original image. The WF utilizes a transfer function applied to the frequency domain representation of the image. After filtering, the inverse FT returns the image to the spatial domain, enhancing its quality as described by Eq. (1).

$$X\left(f_x, f_x\right) = W\left(f_x, f_y\right) * F\left[I\left(x,\ y\right)\right] X\left(x,\ y\right) = F^{\wedge}\ \{-1\}\left[X\left(f_x, f_x\right)\right] \tag{1}$$

The equation describes the process of applying the WF to an image. It first transforms the input image from the spatial domain to the frequency domain using the FT, represented by $F\left[I(\ x,\ y\ )\right]$. Then, the WF, denoted by

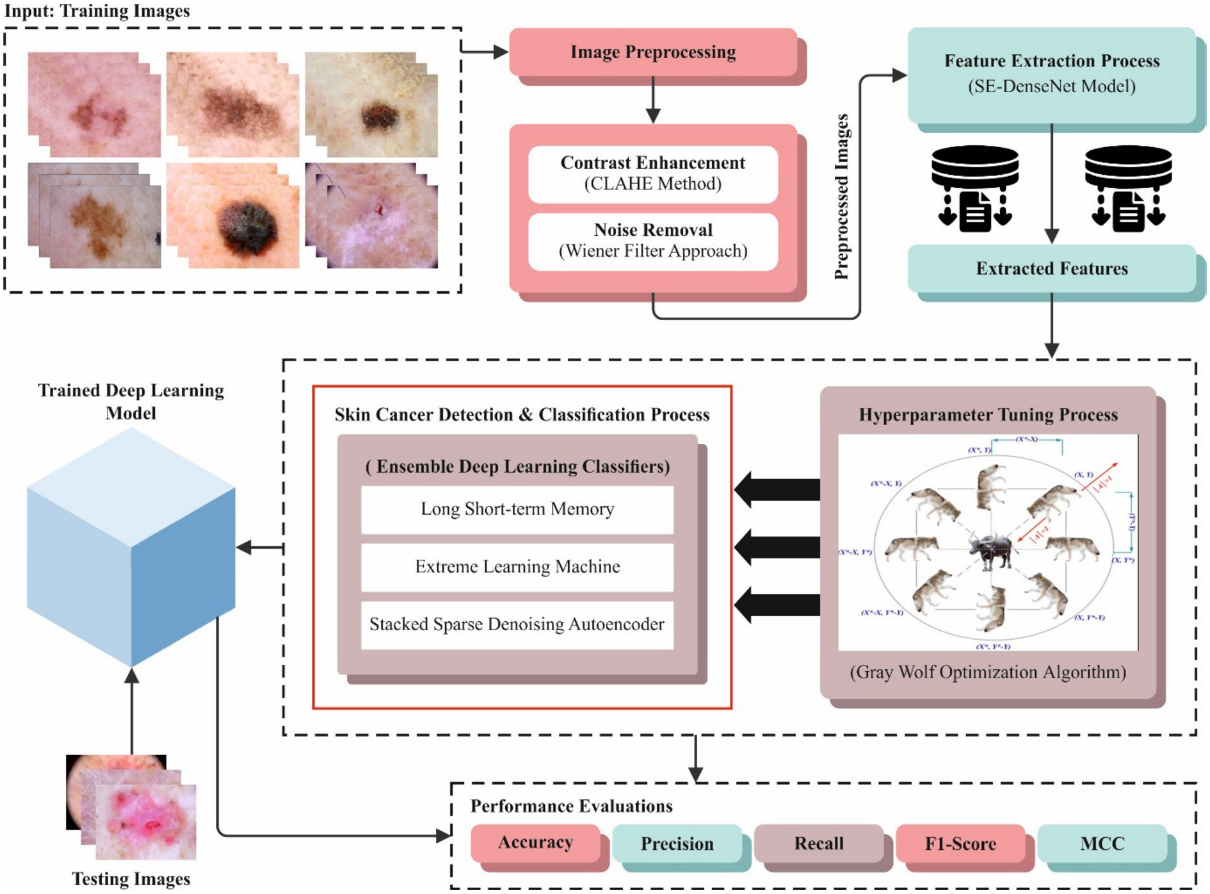

Fig. 1. Overall Workflow of the DSC-EDLMGWO model.

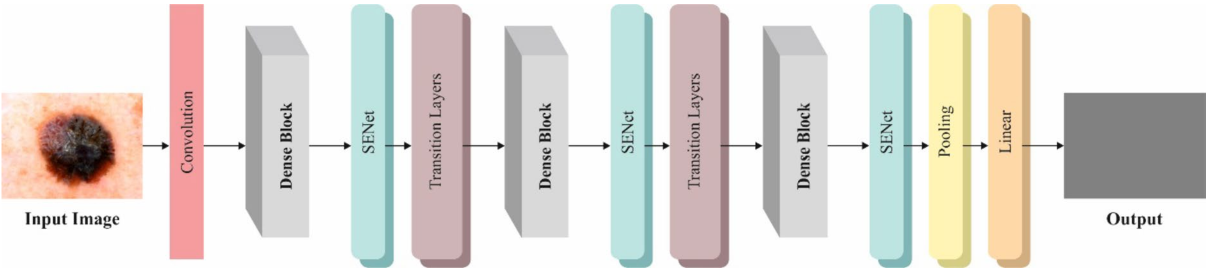

Fig. 2. Structure of SE-DenseNet model.

$W(f_x,\ f_y)$, is applied in the frequency domain to filter the image. Finally, the inverse Fourier Transform, F^{-1}, converts the filtered image back to the spatial domain, resulting in the enhanced output image $X\,(x,\ y)$.

SE-DenseNet-based feature extraction process

Next, the proposed DSC-EDLMGWO model utilizes the fusion of the SE-DenseNet method to extract features[46]. This model was chosen because it can effectively capture hierarchical and contextual features while maintaining computational efficiency. SE-DenseNet improves feature extraction by integrating SE blocks, which adaptively recalibrate feature maps, enhancing the capacity of the method to concentrate on the most informative parts of the image. This results in a more robust feature representation that is highly effective for complex tasks like skin cancer detection. Compared to conventional convolutional networks, SE-DenseNet enhances accuracy and computational efficiency, superiorly handling diverse and intricate image patterns. This makes it ideal for precise image analysis tasks, such as medical image classification. Figure 2 represents the structure of the SE-DenseNet model.

DenseNet is a densely connected neural network (NN) whose network structure is equivalent to ResNet. Initially, a large-scale convolution was performed; formerly, a pooling layer was linked, followed by the Transition

Layer, and the Dense Block was transferred to numerous consecutive subsections. Finally, a fully connected (FC) pooling system gathers the feature mapping of all layers through the feature mapping of each preceding layer within the size of the channel count. All layers in a smaller quantity are recycled, which may decrease the sum of calculation, decrease redundancy, and resolve the problem of gradient disappearance.

The SE module is the calculating component that learns the significance of all channels of an input feature mapping. It enhances the valuable features and diminishes the ineffective characteristics to increase the discrimination capability of the NN. The mathematical expression is given below:

$$U_1 = W^L \otimes f\left(BN\left(W^{L-1} \otimes f\left(BN\left([X_0X_1 \cdots X_{L-1}]\right)\right)\right)\right) \tag{2}$$

During Eq. (2), BN characterizes batch normalization processing; $f(\bullet)$ denotes a function of $ReLU$; W^{L-1} and W^L represent the convolutional kernel of dimensions one by 1, three by 3, correspondingly. Next, the global pooling layer, the squeeze process, is performed. The mathematic representation is demonstrated in Eq. (3):

$$Z_C = F_{sq}(u_c) = \frac{1}{M \times H}\sum\nolimits_{j=1}^{M}\sum\nolimits_{j=1}^{H} u_c(i,j) \tag{3}$$

Meanwhile, u_c and z_c denote the feature graphs. M, H, and C signify the three-dimensional information of the Eigenmatrix U_1. Formerly, the Excitation process is performed; its mathematic standard is exposed in Eq. (4):

$$s_c = F_{ex}(z, W) = \sigma\ (g(z, W)) = \sigma\ (W_2 f(W_1 z_c)) \tag{4}$$

Here, $W_1 \in R^{(C/\beta)\times C}$; $W_2 \in R^{C\times (C/\beta)}$; σ denotes a function of the sigmoid, β refers to the rate of dimensional transformation.

At last, the elements c of the gained scaled matrix s_c and the channels c of the feature graph U_1 are consistent with acquiring the output $Y = [y_1 y_2 \cdots y_c]$. The mathematic basis is presented in Eq. (5):

$$Y = F_{scale}(u_c, s_c) = s_c \cdot u_c \tag{5}$$

During Eq. (5), s_c characterizes the vector gained afterwards SE, and its size is c, u_c symbolizes the feature mapping after the convolutional process, and the channel count is c. SE-DenseNet presented in this study includes the module of SE afterwards, which is the 3 x3 convolution layer of every DenseNet building block. The dotted box is the procedure of X_1 to X_2, and the remaining part handles of X_0 to X_n are equivalent. Through this fusion mechanism, the system cannot simply understand the preserved communication of the new input data; it can also spontaneously learn global information to gain the significance of all channels. Through this fusion mechanism, the system cannot simply comprehend the preserved communication of the new input data; it can also spontaneously learn global information to gain the significance of all channels. This allows the model to adaptively emphasize significant features, enhancing its overall performance and accuracy in complex tasks.

Ensemble of DL models

The classification process is performed using the ensemble of DL models, namely the LSTM, ELM, and SSDA methods. This ensemble model is chosen to improve the robustness and accuracy of the predictions. LSTM is effectual for capturing temporal dependencies in sequential data, which enhances the capability of the method to detect patterns over time. ELM, known for its fast training and strong generalization ability, contributes to reducing computational complexity while maintaining high accuracy. SSDA enhances the technique's capability to handle sparse and noisy data, giving a more refined feature representation. By incorporating these models, the ensemble approach benefits from their complementary strengths, resulting in more accurate, reliable, and efficient classification for complex tasks like skin cancer detection.

LSTM classifier

LSTM is a recurrent NN (RNN) using memory function, which is presented. Compared with conventional RNNs, LSTM includes memory cells, which permit the discernment of valuable data[47]. LSTM comprises four gates for data processing: a memory cell c, the forget f, the input i, and the output gate 0. Formerly, the matrix of forgetting gates f_t is as shown:

$$f_t = \sigma\ (W_f x_t + U_f h_{t-1} + b_f) \tag{6}$$

While σ denotes the sigmoid function, w_f and U_f represent weight matrices of the forget gate, and b_f refers to the matrix of forgetting gate offset parameters. Next, the input gate defines what data must be saved within the present state c_t; formerly, the succeeding is gained:

$$i_t = \sigma\ (W_i x_t + U_i h_{t-1} + b_i) \tag{7}$$

$$\widetilde{c}_t = tanh\,(W_c x_t + U_c h_{t-1} + b_c) \tag{8}$$

Here, i_t denotes the neuron's input gate matrix at t^{th} time, c_t refers to the neuron's cell candidate state matrix at t^{th} time; W_j and U_i represent input gate weighted matrix; b_i denotes the matrix of input gate offset parameters; W_c and U_c are the cell candidate state, and b_c stands for the cell state. From Eqs. (6)- (8), the matrix of unit state c_t is expressed below:

$$c_t = f_t \otimes\ c_{t-1} + i_t \otimes\ \tilde{c}_t \tag{9}$$

Whereas $\otimes$ denotes the matrix of a dot product. At last, the output gate defines the output control of cell state c_t to h_t:

$$0_t = \sigma\ \left(W_o x_t + U_o h_{t-1} + b_o\right) \tag{10}$$

$$h_t = o_t \otimes\ tanhc_t \tag{11}$$

Now, o_t denotes the neuron's output gate matrix at t^{th} time , W_o and U_o characteristics output gate weighted matrix; b_0 signifies the output gate, and h_t denotes the neuron's output matrix at t time. Additionally, LSTM determines the difficulties of the longer-range dependence nature of RNNs, making it appropriate for short-term memory time-series regression tasks.

ELM classifier

The ELM is a fundamental and effectual feedforward NN with a unique hidden layer (SLFN)[48]. It provides an analytical model for training the system. When the node counts and HL activation function are stated, the particular optimum solution is attained through training data.

While ELM's inputs and outputs, they are specified as shown:

$$X = \begin{bmatrix} x_{11} & \ldots & x_{1Q} \\ x_{n1} & \ldots & x_{nQ} \end{bmatrix}; T = \begin{bmatrix} t_{11} & \ldots & t_{1Q} \\ t_{m1} & \ldots & t_{mQ} \end{bmatrix} \tag{12}$$

Meanwhile, n and m represent the sizes of an input and output matrix. The weights were fixed at random between the HL and the input layer:

$$W = \begin{bmatrix} w_{11} & \ldots & w_{1\ m} \\ w_{m1} & \ldots & w_{nm} \end{bmatrix} \tag{13}$$

Where w_{ij} characterizes the weights among the j^{th} layer and the i^{th} neuron. Its mathematical equation is expressed below:

$$\beta\ = \begin{bmatrix} \beta_{\ 11} & \ldots & \beta_{\ 1\ m} \\ \beta_{\ l1} & \ldots & \beta_{\ km} \end{bmatrix} \tag{14}$$

Here, $\beta_{\ ij}$ characterizes the weights among the j^{Th} HL and k^{th} neurons. Its formulation is given below:

$$B = \left[b_1\, b_2\ \ldots\ b_n\right]' \tag{15}$$

The ELM selects the activation function $g\left(x\right)$. Based on this, the T is stated as shown:

$$T = \begin{bmatrix} t_{11} & \ldots & t_{1Q} \\ t_{m1} & \ldots & t_{mQ} \end{bmatrix}_{m\times\ Q} \tag{16}$$

Every column vector of matrix T is as shown:

$$t_j = \begin{bmatrix} t_{1j} \\ t_{2j} \\ t_{mj} \end{bmatrix} = \begin{bmatrix} \sum\ {}_{i=1}^{l}\beta_{\ i1} g\left(w_j x_j + b_i\right) \\ \sum\ {}_{i=1}^{l}\beta_{\ i2} g\left(w_j x_j + b_i\right) \\ \ldots \\ \sum\ {}_{i=1}^{l}\beta_{\ im} g\left(w_j x_j + b_i\right) \end{bmatrix}; [j \ldots\ (i = 1{,}2{,}3,\ \ldots\ , Q) \tag{17}$$

From Eqs. (16) and (17), $H\beta\ = T'$ is attained.

Meanwhile, T' denotes the transpose of T, and H represents the output. The least-square model is used to compute the values of the weighted matrix β .

$$\beta\ = H^{\dagger} T' \tag{18}$$

Whereas $H^{\dagger}$ denotes the Moore-Penrose general inverse of matrix H. The term of regularization is added to the β for the enhancement. After the HL neuron counts are lower than the training sample counts, β is stated as:

$$\beta\ = \left(\frac{I}{\lambda} + H'\ H\right)^{-1} H'\ T' \tag{19}$$

Here: $\beta\ '\beta\ = I$ and λ refers to the regularization coefficient. Once the hidden layer node counts are more significant than the training sample counts, β is stated as:

$$\beta\ = H' \left(\frac{I}{\lambda} + HH'\right)^{-1} T' \tag{20}$$

SSDA classifier

AE are self-directed NNs. In principle, both input and output are expected to be similar. Nevertheless, it is established that when the input toward AE is noisy, and the output is clear, the weights of the AE are more substantial[49]. Nevertheless, SSDA-based denoising is recursive and transduces naturally. To train the SSDA learning for denoising from a larger volume of training data, an input to the SSDA is noisy instances, and the outputs are consistent, clear samples. In testing, the noise samples are provided as input, and a clean sample is required.

One experimentally stated benefit is that one is not required to alter the AE training model based on the noise method in some models. Training data needs to be contaminated by the kind of noise that must be cleaned. Dual SSDAs need to be learned. The similar uses for additional types of noise, namely speckle, impulse, and so on. SSDA-based denoising might be intensely dependent on training data; it assumes the testing data is equivalent to the training data. There is no lack of natural images online, so making a larger collection of training is possible. SSDA trained on natural images provides the worst performance in analytical imaging conditions. Therefore, the AE declines to simplify the hidden modalities. Practically, even though fine-tuning an essential amount of data is needed.

GWO-based hyperparameter tuning process

Finally, the GWO approach optimally adjusts the ensemble DL models' hyperparameter values, improving classification performance[50]. This method is chosen for its robust capability to explore the search space efficiently and find optimal hyperparameters in DL methods. Inspired by the social hunting behaviour of gray wolves, GWO effectually balances exploration and exploitation, avoiding local minima and ensuring better global search results. This process is more effectual than conventional methods like grid and random search, as it dynamically adjusts to the complexity of the model's hyperparameter space. The flexibility of the GWO model allows it to optimize multiple hyperparameters simultaneously, which is significant for enhancing the accuracy and generalization of complex models. Furthermore, it significantly mitigates computational costs by converging faster, making it an ideal choice for large-scale DL tasks. The use of GWO assists in fine-tuning the models for improved performance and robustness in real-world applications. Figure 3 demonstrates the steps involved in the GWO method.

GWO is stimulated by cooperative gray wolf hunting behaviour. Usually, these wolf packs have a hierarchical framework describing social dynamics and comprise a group's beta, omega, and alpha members. The alpha wolf is the highest part of this hierarchy, simulating the significant role inside the pack, and is dependable for pattern movements, periods of rest, and dictating hunting approaches. The GWO model is advanced with the consideration of the social behaviour of the wolf. The alpha wolf signifies the fundamental solution in this model, whereas the gamma and beta wolves denote the two best solutions. In the gray wolf's searching behaviour, they work collaboratively to encircle their prey during hunting. This cooperative strategy enhances the efficiency of locating the prey. The model leverages these social interactions to improve search accuracy and optimization. The mathematical method for this turning behaviour, Eqs. (21) and (22) are represented.

$$\vec{D}_\alpha = \left|\vec{C}_1 \cdot \vec{X}_\alpha - \vec{X}\right|, \vec{D}_\beta = \left|\vec{C} \cdot \vec{X} - \vec{X}\right|, \vec{D}_\delta = \left|\vec{C}_3 \cdot \vec{X}_\delta - \vec{X}\right| \tag{21}$$

$$\vec{X}_1 = \vec{X}_\alpha - \vec{A}_1 \cdot \vec{D}_\alpha, \vec{X}_2 = \vec{X}_\beta - \vec{A}_2 \cdot \vec{D}_\beta, \vec{X}_3 = \vec{X}_\delta - \vec{A}_3 \cdot \vec{D}_\delta \tag{22}$$

In the current scenario, the symbol t signifies the number of repetitions, whereas C and A represent vector coefficients. X and P denote the gray and prey wolves' position vectors individually. The vector determination of A and C follows the computations summarized in Eqs. (23) and (24).

$$\vec{A} = 2\vec{a} \cdot \vec{r}_1 - \vec{a} \tag{23}$$

$$\vec{C} = 2\vec{r}_2 \tag{24}$$

As $\vec{a}$ linearly reduces from 2 to 0 throughout iterations, r_1 and r_2 signify random vectors. The delta and beta wolves have adequate awareness of the possible prey location; subsequently, the earlier three more excellent solutions are conserved, captivating other search agent omegas to modify their locations related to the best search assistant, as defined in Eqs. (25) to (31).

$$\vec{D}_\alpha = \left|\vec{C}_1 \cdot \vec{X}_\alpha - \vec{X}\right| \tag{25}$$

$$\vec{D}_\beta = \left|\vec{C}_2 \cdot \vec{X}_\beta - \vec{X}\right| \tag{26}$$

$$\vec{D}_\delta = \left|\vec{C}_3 \cdot \vec{X}_\delta - \vec{X}\right| \tag{27}$$

$$\vec{X}_1 = \vec{X}_\alpha - \vec{A}_1 \cdot \vec{D}_\alpha \tag{28}$$

$$\vec{X}_2 = \vec{X}_\beta - \vec{A}_2 \cdot \vec{D}_\beta \tag{29}$$

$$\vec{X}_3 = \vec{X}_\delta - \vec{A}_2 \cdot \vec{D}_\delta \tag{30}$$

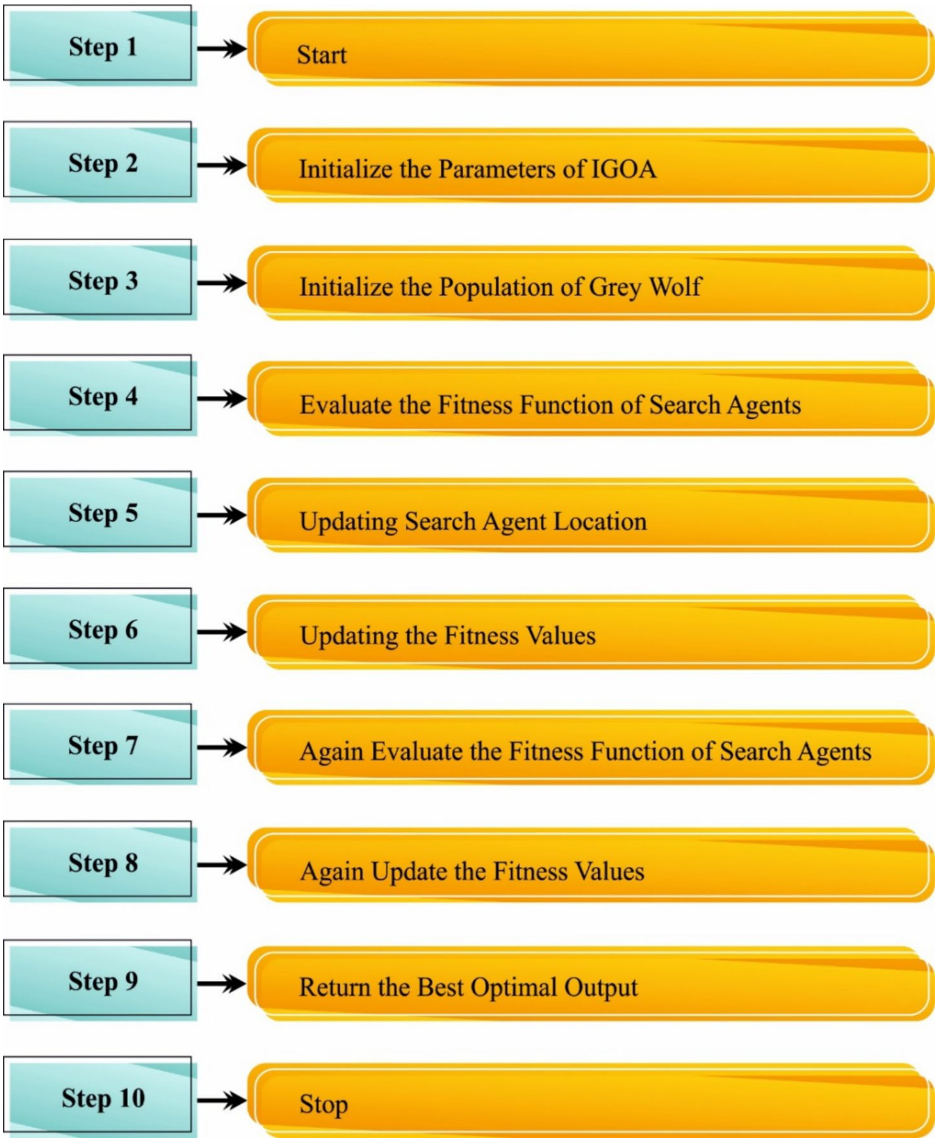

Fig. 3. Steps involved in the GWO methodology.

$$\vec{X}\left(i+1\right)=\frac{\vec{X}_1+\vec{X}_2+\vec{X}_3}{3} \tag{31}$$

The final position is randomly determined within a circle defined by the research area's beta, delta, and alpha positions. These positions are primarily implemented to estimate the location of the prey. The process helps refine the wolves' position relative to the prey. Based on this, another wolf randomly updates its position to improve the hunt. This randomness confirms diverse approaches to locating the prey. The GWO model originates a fitness function (FF) for achieving an enhanced classification outcome. It states an optimistic numeral to signify the more excellent result of the candidate solution. Here, the reduction of the classifier rate of error has been measured as FF. Its mathematical formulation is demonstrated in the below Eq. (32).

$$fitness\left(x_i\right)=ClassifierErrorRate\left(x_i\right)=\frac{No.\,of\ misclassified\ samples}{Total\ no.\,of\ samples}\times\ 100 \tag{32}$$

Performance analysis

The performance evaluation of the DSC-EDLMGWO approach is confirmed under the HAM10000 dataset[51]. The dataset contains 10,082 samples under seven classes, as shown in Table 1. Figure 4 represents the sample images.

Figure 5 presents the classifier results of the DSC-EDLMGWO methodology on the HAM10000 database. Figure 5a and b shows the confusion matrices with correct recognition and classification of all classes under 70%TRPH and 30%TSPH. Figure 5c demonstrates the PR values, signifying superior performance through all

HAM10000 Database		
Description	**Classes**	**No. of Instances**
"Actinic Keratosis"	AKIEC	327
"Basal Cell Carcinoma"	BCC	541
"Benign Keratosis"	BKL	1099
"Dermatofibroma"	DF	155
"Melanocytic Nevus"	NV	6705
"Melanoma"	MEL	1113
"Vascular"	VASC	142
Total Number of Instances		**10,082**

Table 1. Details of the HAM10000 dataset.

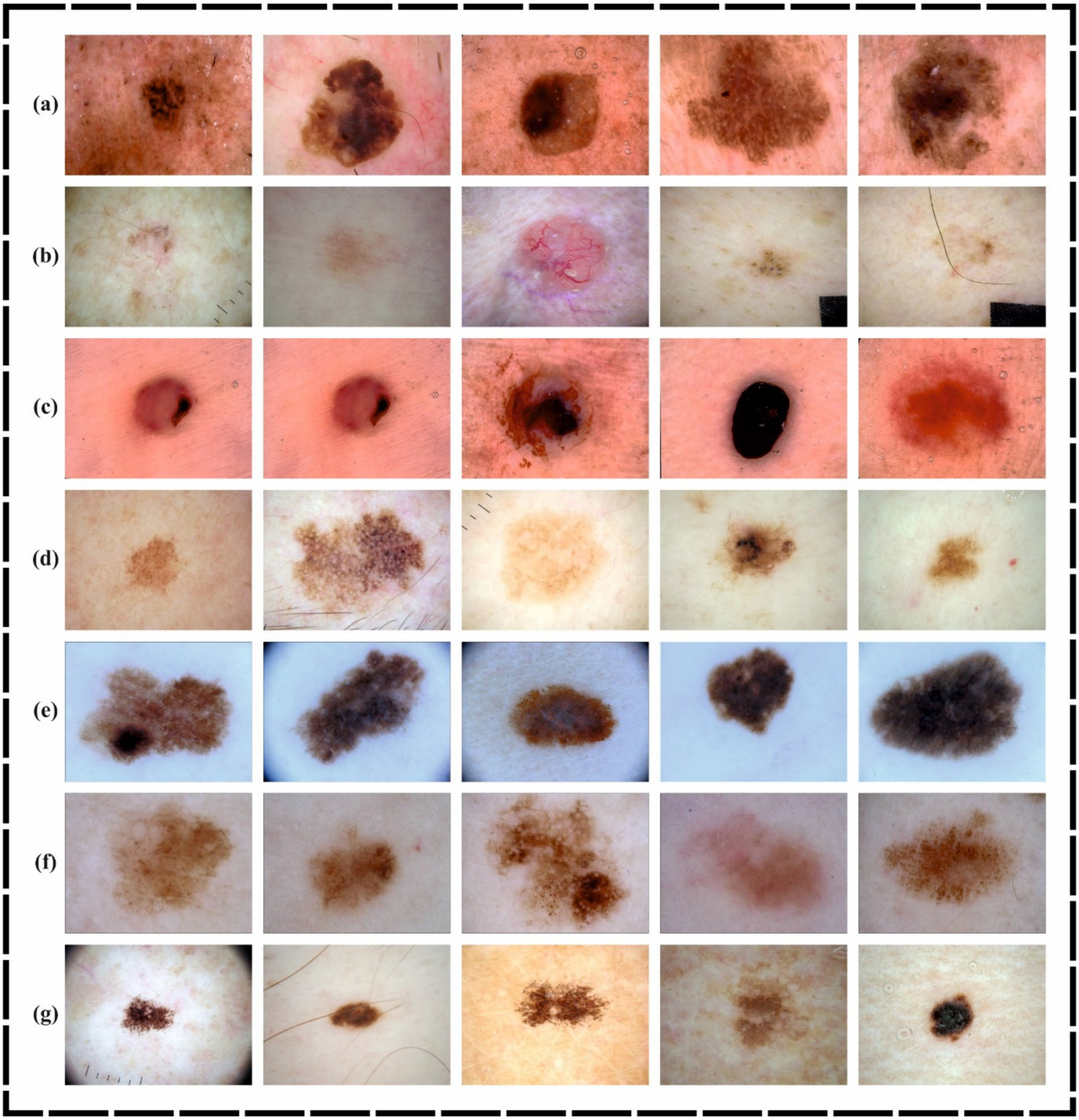

Fig. 4. Sample images (**a**) Actinic Keratosis, (**b**) Basal Cell Carcinoma, (**c**) Benign Keratosis, (**d**) Dermatofibroma, (**e**) Melanocytic Nevus, (**f**) Melanoma, and (**g**) Vascular.

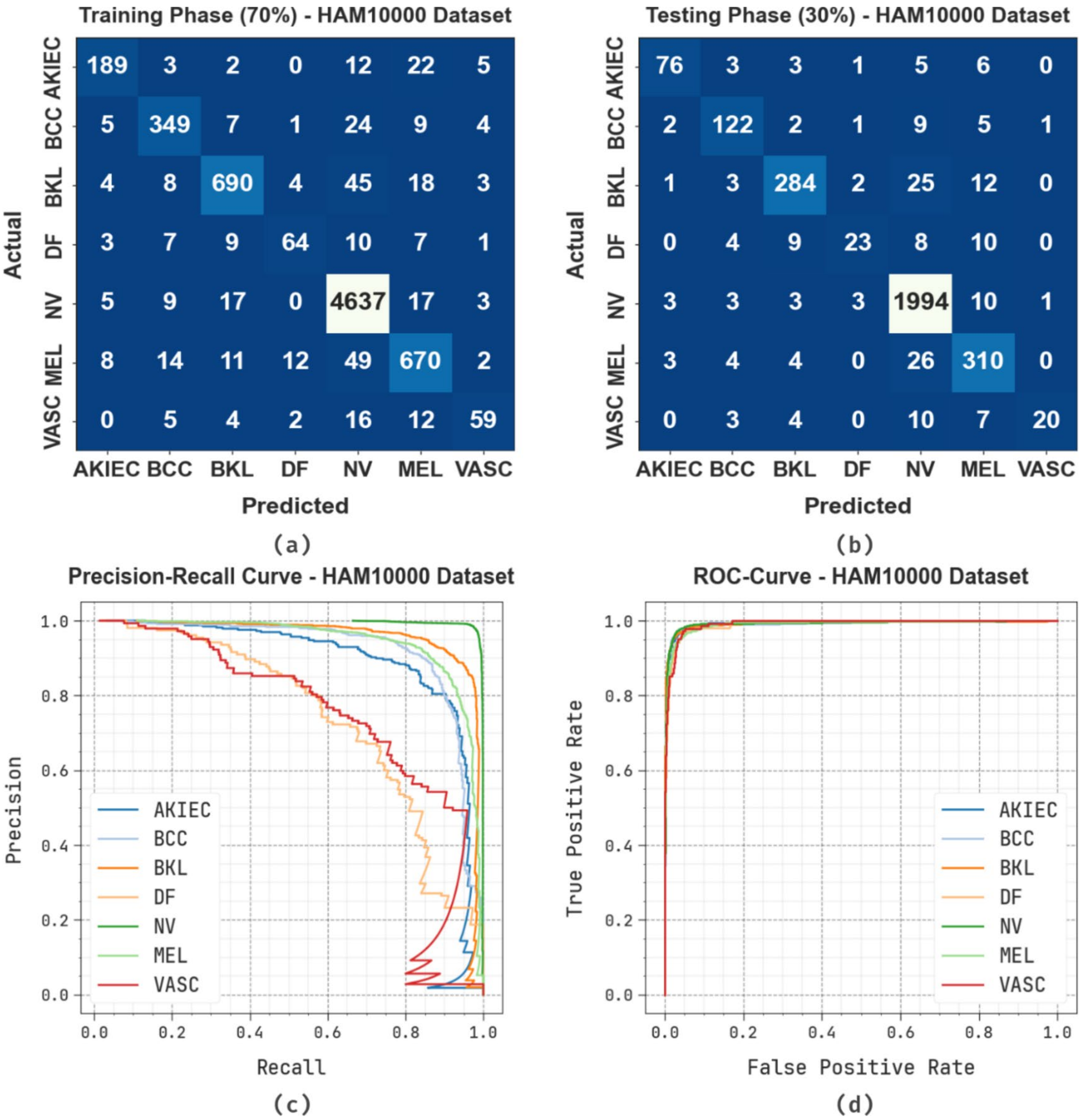
Training Phase (70%) - HAM10000 Dataset

Actual \ Predicted	AKIEC	BCC	BKL	DF	NV	MEL	VASC
AKIEC	189	3	2	0	12	22	5
BCC	5	349	7	1	24	9	4
BKL	4	8	690	4	45	18	3
DF	3	7	9	64	10	7	1
NV	5	9	17	0	4637	17	3
MEL	8	14	11	12	49	670	2
VASC	0	5	4	2	16	12	59

(a)

Testing Phase (30%) - HAM10000 Dataset

Actual \ Predicted	AKIEC	BCC	BKL	DF	NV	MEL	VASC
AKIEC	76	3	3	1	5	6	0
BCC	2	122	2	1	9	5	1
BKL	1	3	284	2	25	12	0
DF	0	4	9	23	8	10	0
NV	3	3	3	3	1994	10	1
MEL	3	4	4	0	26	310	0
VASC	0	3	4	0	10	7	20

(b)

Precision-Recall Curve - HAM10000 Dataset

(c)

ROC-Curve - HAM10000 Dataset

(d)

Fig. 5. HAM10000 database (**a**-**b**) Confusion matrix, (**c**-**d**) PR and ROC curves.

class labels. At the same time, Fig. 5d shows the ROC values, demonstrating proficient results with better ROC analysis for different classes.

In Table 2; Fig. 6, the skin cancer detection of the DSC-EDLMGWO approach is illustrated on the HAM10000 database. The results reported that the DSC-EDLMGWO approach accurately discriminated all the samples. On 70%TRPH, the DSC-EDLMGWO approach presents an average $accu_y$ of 98.38%, $prec_n$ of 87.02%, $reca_l$ of 81.13%, $F1_{score}$ of 83.81%, and MCC of 82.67%. In addition, on 30%TSPH, the DSC-EDLMGWO method presents an average $accu_y$ of 98.15%, $prec_n$ of 88.13 $reca_l$ of 75.69%, $F1_{score}$ of 80.09%, and MCC of 79.52%.

Figure 7 establishes the training (TRA) $accu_y$ and validation (VAL) $accu_y$ analysis of the DSC-EDLMGWO technique on the HAM10000 database. The $accu_y$ analysis is computed across the range of 0–50 epochs. The figure highlights that the TRA and VAL $accu_y$ analysis displays a rising trend, which informed the capacity of the DSC-EDLMGWO methodology with higher outcomes across several iterations.

Figure 8 shows the TRA loss (TRALOS) and VAL loss (VALLOS) analysis of the DSC-EDLMGWO approach on the HAM10000 database. The loss values are calculated over the range of 0–50 epochs. The TRALOS and VALLOS values exemplify a decreasing trend, notifying the DSC-EDLMGWO methodology's ability to balance a trade-off between generalization and data fitting.

Table 3; Fig. 9 study the comparison outcomes of the DSC-EDLMGWO approach on the HAM10000 database with the existing models[52–55]. The results highlighted that the MAFCNN-SCD, HARTS, Kernel-ELM, SDDLNN-MobileNetV2, and DL-SCL approaches have reported worse performance. Meanwhile, Ensemble CNN + SVM and MobileNet V2-LSTM techniques have achieved closer outcomes. Simultaneously, the DSC-

Class Labels	$Accu_y$	$Prec_n$	$Reca_l$	$F1_{score}$	MCC
TRPH (70%)					
AKIEC	99.02	88.32	81.12	84.56	84.14
BCC	98.64	88.35	87.47	87.91	87.19
BKL	98.13	93.24	89.38	91.27	90.25
DF	99.21	77.11	63.37	69.57	69.51
NV	97.07	96.75	98.91	97.82	93.40
MEL	97.44	88.74	87.47	88.10	86.67
VASC	99.19	76.62	60.20	67.43	67.53
Average	**98.38**	**87.02**	**81.13**	**83.81**	**82.67**
TSPH (30%)					
AKIEC	99.11	89.41	80.85	84.92	84.57
BCC	98.68	85.92	85.92	85.92	85.22
BKL	97.75	91.91	86.85	89.31	88.10
DF	98.74	76.67	42.59	54.76	56.60
NV	96.50	96.00	98.86	97.41	92.09
MEL	97.12	86.11	89.34	87.69	86.09
VASC	99.14	90.91	45.45	60.61	63.95
Average	**98.15**	**88.13**	**75.69**	**80.09**	**79.52**

Table 2. Skin cancer detection of DSC-EDLMGWO model on HAM10000 database.

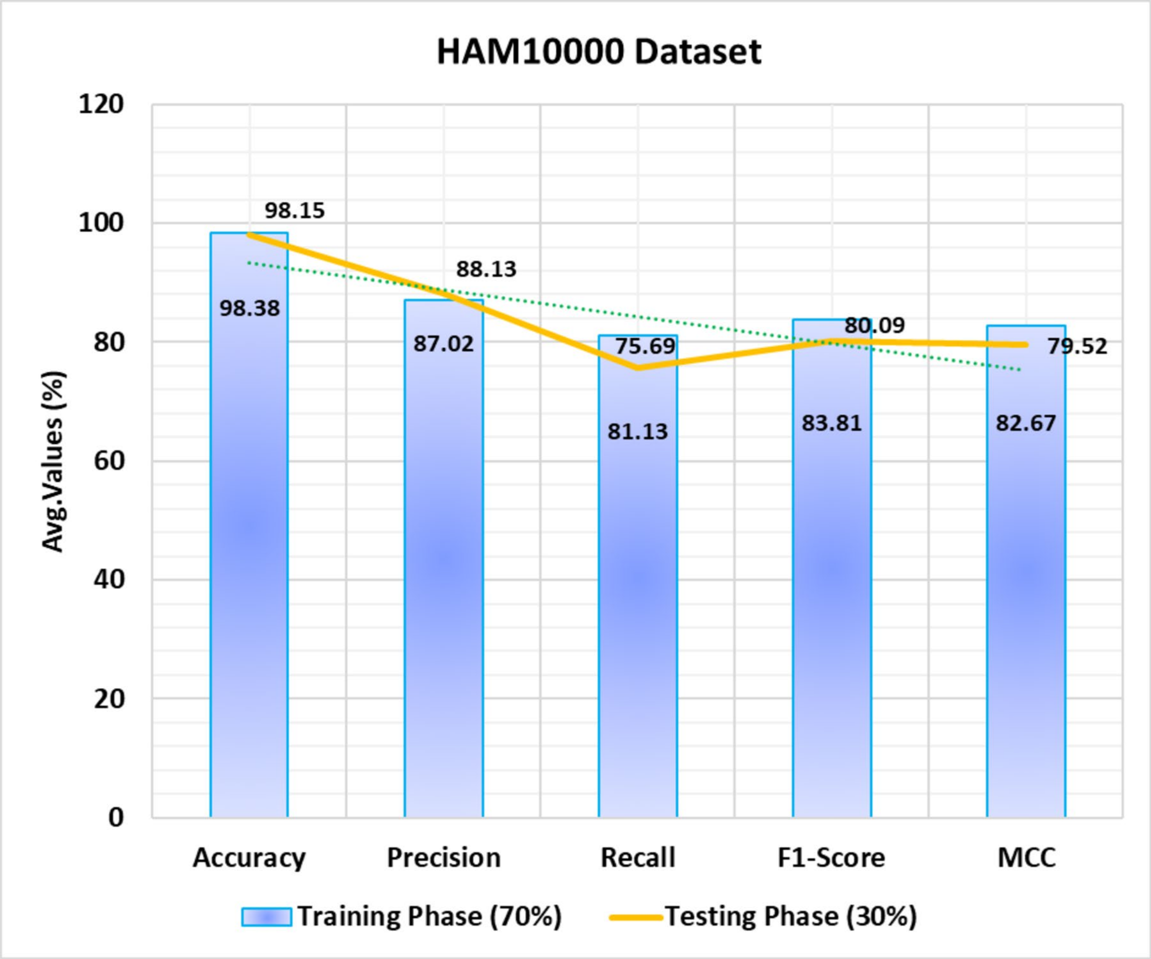

Fig. 6. Average of DSC-EDLMGWO model on HAM10000 database.

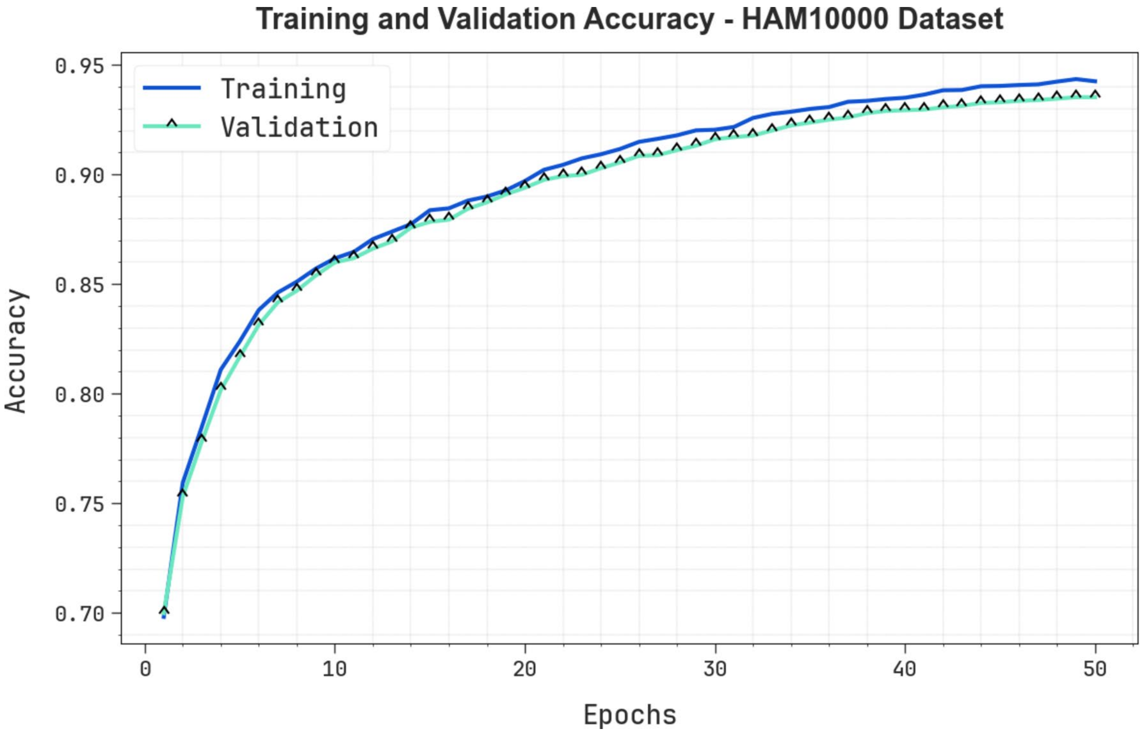

Fig. 7. $Accu_y$ analysis of the DSC-EDLMGWO model on the HAM10000 database.

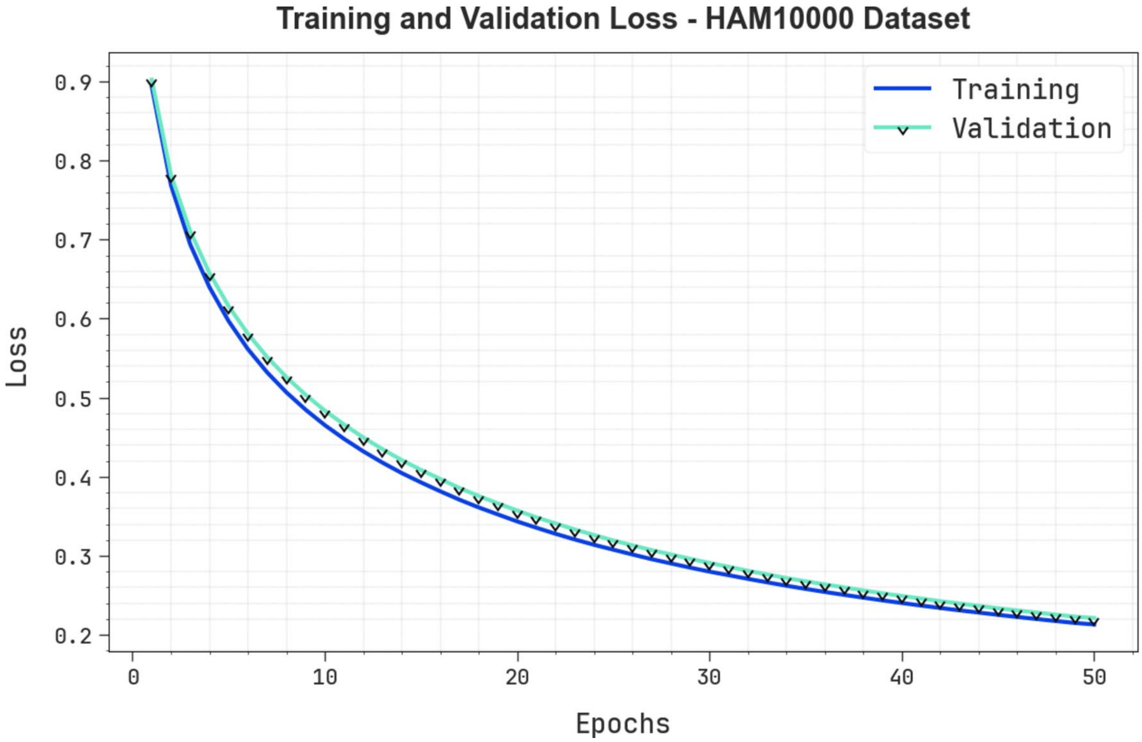

Fig. 8. Loss graph of DSC-EDLMGWO model on HAM10000 database.

EDLMGWO methodology reported higher performance with superior $prec_n$, $reca_l$, $accu_y$, and $F1_{score}$ of 87.02%, 81.13%, 98.38%, and 83.81%, correspondingly.

Table 4; Fig. 10 illustrate the computational time (CT) analysis of the DSC-EDLMGWO technique with existing methods under HAM10000 dataset. Different models exhibit varying CTs, such as the DSC-EDLMGWO

HAM10000 Database				
Framework	$Accu_y$	$Prec_n$	$Recal_l$	$F1_{score}$
DSC-EDLMGWO	98.38	87.02	81.13	83.81
Ensemble CNN + SVM	96.52	85.88	76.50	80.64
MAFCNN-SCD	92.25	82.51	80.77	77.01
HARTS Method	90.78	80.59	80.95	79.53
Kernel-ELM	88.07	84.86	78.48	79.05
MobileNet V2-LSTM	96.13	78.75	78.27	76.50
SDDLNN-MobileNetV2	94.88	77.41	76.90	77.55
DL-SCL Method	93.10	79.78	78.21	79.55

Table 3. Comparative analysis of the DSC-EDLMGWO model on the HAM10000 database[52–55].

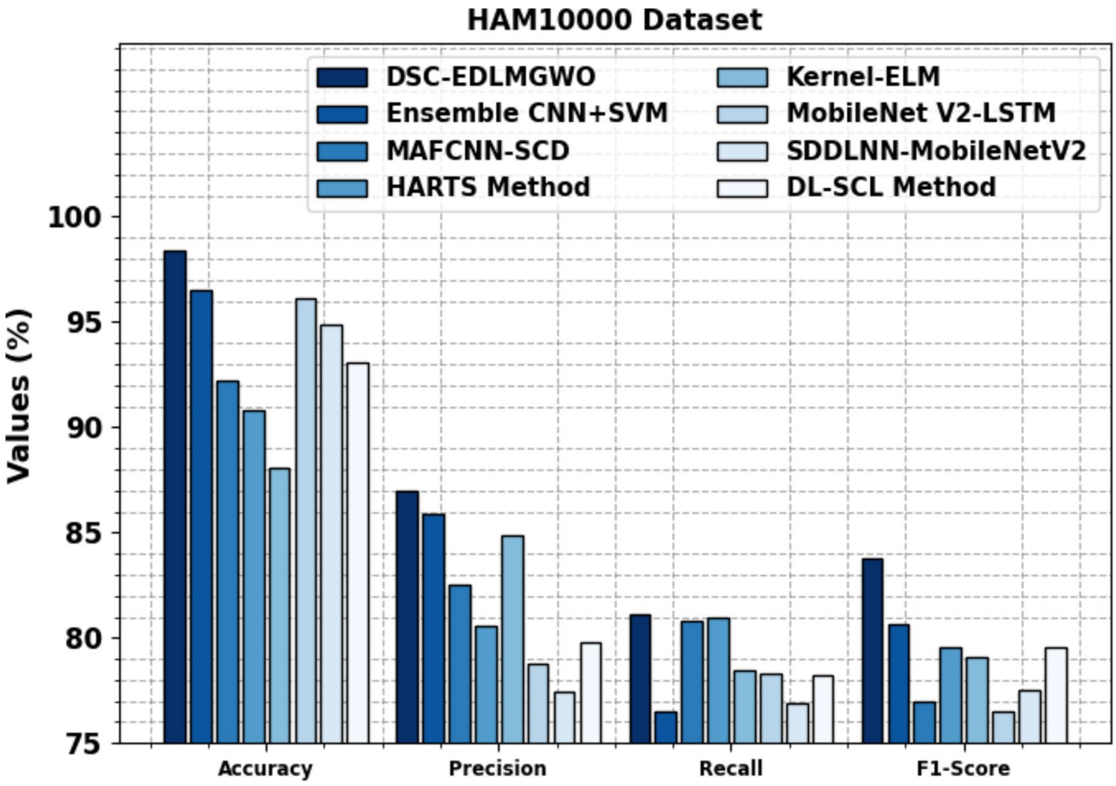

Fig. 9. Comparative analysis of the DSC-EDLMGWO model on the HAM10000 database.

HAM10000 Database	
Framework	**CT (sec)**
DSC-EDLMGWO	4.96
Ensemble CNN + SVM	8.21
MAFCNN-SCD	6.53
HARTS Method	7.50
Kernel-ELM	7.79
MobileNet V2-LSTM	9.42
SDDLNN-MobileNetV2	6.27
DL-SCL Method	8.82

Table 4. CT evaluation of the DSC-EDLMGWO model on the HAM10000 dataset.

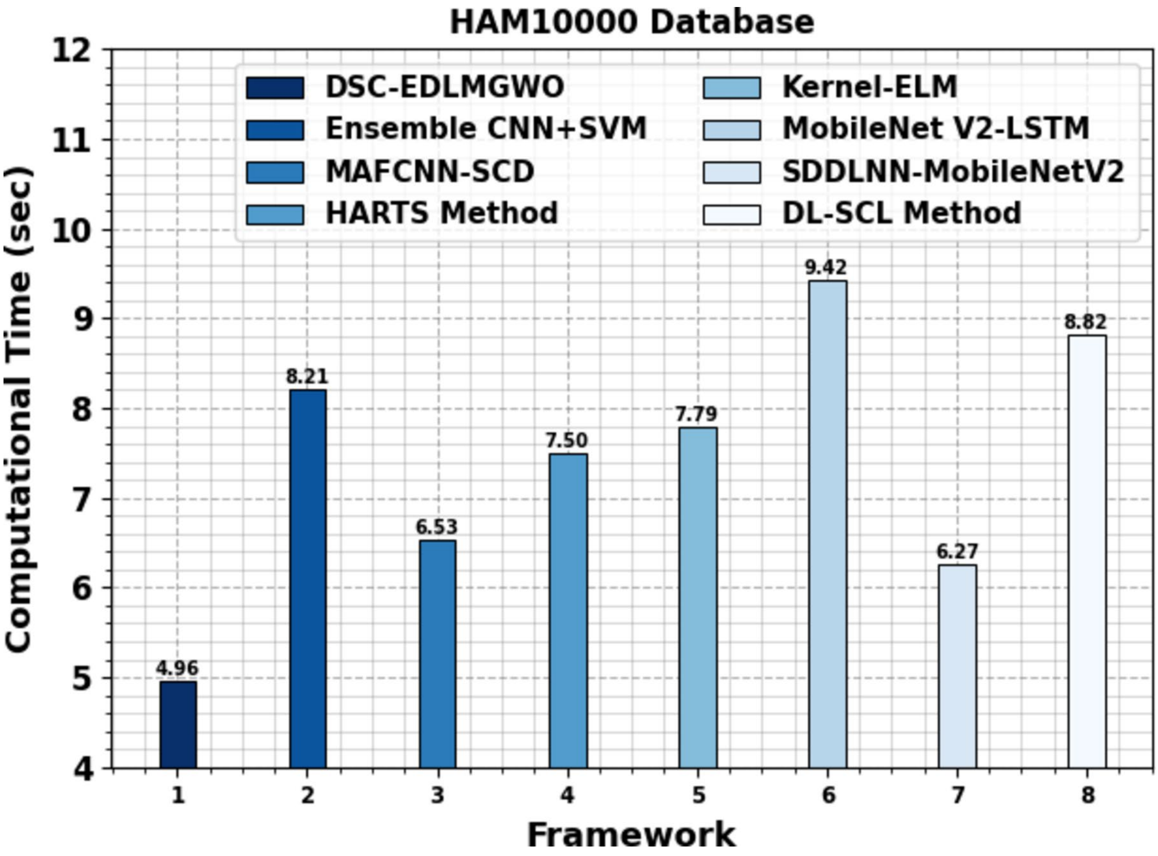

Fig. 10. CT evaluation of the DSC-EDLMGWO model on the HAM10000 dataset.

Classes	Labels	Image Count
"Actinic Keratosis"	Class1	110
"Basal Cell Carcinoma"	Class2	370
"Dermatofibroma"	Class3	90
"Melanoma"	Class4	430
"Nevus"	Class5	350
"Pigmented Benign Keratosis"	Class6	460
"Seborrheic Keratosis"	Class7	70
"Squamous Cell Caricinoma"	Class8	180
"Vascular Lesion"	Class9	130
Total Number Images		**2190**

Table 5. Details of ISIC database.

method with 4.96 s, Ensemble CNN + SVM at 8.21 s, MAFCNN-SCD at 6.53 s, HARTS at 7.50 s, Kernel-ELM at 7.79 s, and MobileNet V2-LSTM at 9.42 s. SDDLNN-MobileNetV2 performs at 6.27 s, while DL-SCL method takes 8.82 s, emphasizing the trade-offs between efficiency and accuracy in diverse frameworks.

Also, the performance evaluation of the DSC-EDLMGWO methodology is verified under the ISIC database[56]. The database contains 2190 images under nine classes, as represented in Table 5.

Figure 11 illustrates the classifier results of the DSC-EDLMGWO approach on the ISIC database. Figure 11a and b displays the confusion matrices with correct classification and recognition of all classes under 70%TRPH and 30%TSPH. Figure 11c demonstrates the PR values, specifying superior performance through all class labels. In addition, Fig. 11d shows the ROC values, indicating capable outcomes with maximal ROC analysis for dissimilar class labels.

In Table 6; Fig. 12, the skin cancer detection of the DSC-EDLMGWO method is illustrated on the ISIC database. The results reported that the DSC-EDLMGWO method correctly discriminated each of the samples. On 70%TRPH, the DSC-EDLMGWO methodology presents an average $accu_y$ of 97.90%, $prec_n$ of 89.08%, $reca_l$ of 83.92%, $F1_{score}$ of 86.15%, and MCC of 85.15%. Moreover, on 30%TSPH, the DSC-EDLMGWO

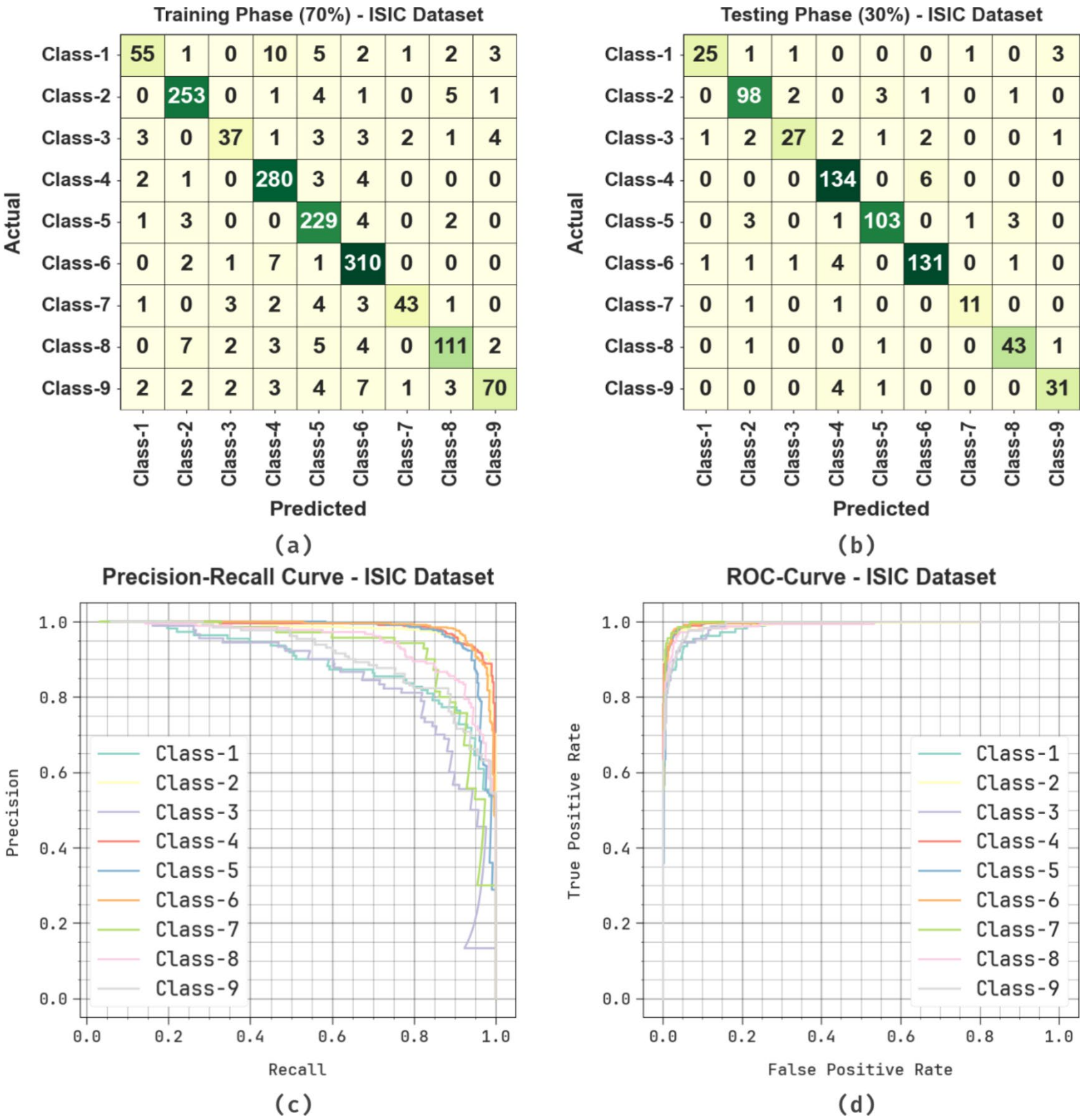

Training Phase (70%) - ISIC Dataset

	Class-1	Class-2	Class-3	Class-4	Class-5	Class-6	Class-7	Class-8	Class-9
Class-1	55	1	0	10	5	2	1	2	3
Class-2	0	253	0	1	4	1	0	5	1
Class-3	3	0	37	1	3	3	2	1	4
Class-4	2	1	0	280	3	4	0	0	0
Class-5	1	3	0	0	229	4	0	2	0
Class-6	0	2	1	7	1	310	0	0	0
Class-7	1	0	3	2	4	3	43	1	0
Class-8	0	7	2	3	5	4	0	111	2
Class-9	2	2	2	3	4	7	1	3	70

Testing Phase (30%) - ISIC Dataset

	Class-1	Class-2	Class-3	Class-4	Class-5	Class-6	Class-7	Class-8	Class-9
Class-1	25	1	1	0	0	0	1	0	3
Class-2	0	98	2	0	3	1	0	1	0
Class-3	1	2	27	2	1	2	0	0	1
Class-4	0	0	0	134	0	6	0	0	0
Class-5	0	3	0	1	103	0	1	3	0
Class-6	1	1	1	4	0	131	0	1	0
Class-7	0	1	0	1	0	0	11	0	0
Class-8	0	1	0	0	1	0	0	43	1
Class-9	0	0	0	4	1	0	0	0	31

Fig. 11. ISIC Database (**a**-**b**) Confusion matrix, (c-d) PR and ROC curves.

methodology presents an average $accu_y$ of 98.17%, $prec_n$ of 90.16%, $reca_l$ of 88.44%, $F1_{score}$ of 89.19%, and MCC of 88.19%.

In Fig. 13, TRA $accu_y$ and VAL $accu_y$ outcomes of the DSC-EDLMGWO technique on the ISIC database are established. The $accu_y$ analysis is computed across the range of 0–50 epochs. The figure highlights that the TRA and VAL $accu_y$ analysis demonstrates an increasing trend that notified the capacity of the DSC-EDLMGWO methodology with maximal outcomes through multiple iterations.

In Fig. 14, the TRALOS and VALLOS curves of the DSC-EDLMGWO technique on the ISIC database are demonstrated. The loss values are computed within the range of 0–50 epochs. The TRALOS and VALLOS values exemplify a diminishing tendency, notifying the capacity of the DSC-EDLMGWO methodology to balance a trade-off between generalization and data fitting.

Table 7; Fig. 15 compare the outcomes of the DSC-EDLMGWO approach on the ISIC database with those of the existing techniques. The outcomes emphasized that the VGG19, Ensemble CNN-EfficientNet, ResNet-152, Efficient-B7, DenseNet169, and SCC-DCNNTLM models have reported inferior performance. Meanwhile, the DSCC-Net SMOTE Tomek approach has accomplished closer outcomes. Besides, the DSC-EDLMGWO approach reported maximum performance with maximal $prec_n$, $reca_l$, $accu_y$, and $F1_{score}$ of 90.16%, 88.44%, 89.19%, and 98.17%, respectively.

Table 8; Fig. 16 demonstrates the CT evaluation of the DSC-EDLMGWO technique with existing models under ISIC dataset. The DSC-EDLMGWO method has a CT of 7.12 s, while the VGG19 approach takes 12.64 s. MAFCNN-SCD has a CT of 14.43 s, and the Ensemble CNN-EfficientNet framework takes 14.02 s. ResNet-152 performs at 14.51 s, Efficient-B7 at 10.96 s, and DenseNet169 model at 12.34 s. SCC-DCNNTLM achieves a CT

Class Labels	$Accu_y$	$Prec_n$	$Reca_l$	$F1_{score}$	MCC
TRPH (70%)					
Class-1	97.85	85.94	69.62	76.92	76.27
Class-2	98.17	94.05	95.47	94.76	93.65
Class-3	98.37	82.22	68.52	74.75	74.24
Class-4	97.59	91.21	96.55	93.80	92.36
Class-5	97.46	88.76	95.82	92.15	90.73
Class-6	97.46	91.72	96.57	94.08	92.51
Class-7	98.83	91.49	75.44	82.69	82.50
Class-8	97.59	88.80	82.84	85.71	84.46
Class-9	97.78	87.50	74.47	80.46	79.58
Average	**97.90**	**89.08**	**83.92**	**86.15**	**85.15**
TSPH (30%)					
Class-1	98.78	92.59	80.65	86.21	85.80
Class-2	97.56	91.59	93.33	92.45	91.01
Class-3	98.02	87.10	75.00	80.60	79.81
Class-4	97.26	91.78	95.71	93.71	91.99
Class-5	97.87	94.50	92.79	93.64	92.36
Class-6	97.41	93.57	94.24	93.91	92.27
Class-7	99.39	84.62	84.62	84.62	84.30
Class-8	98.78	89.58	93.48	91.49	90.86
Class-9	98.48	86.11	86.11	86.11	85.31
Average	**98.17**	**90.16**	**88.44**	**89.19**	**88.19**

Table 6. Skin cancer detection of DSC-EDLMGWO model on ISIC database.

of 11.71 s, while DSCC-Net SMOTE Tomek has the highest CT at 14.62 s, illustrating the discrepancy in model efficiency across diverse frameworks.

Conclusion

This manuscript presented a DSC-EDLMGWO method. The proposed DSC-EDLMGWO method relies upon skin cancer detection in biomedical imaging. At first, the presented DSC-EDLMGWO model involved an image preprocessing stage at two levels: contract enhancement using the CLAHE method and noise removal using the WF model. Next, the proposed DSC-EDLMGWO model utilized the fusion of the SE-DenseNet method to extract a feature. The ensemble of DL models, namely the LSTM, ELM, and SSDA methods, was employed for the classification process. Finally, the GWO method optimally adjusts the ensemble DL models' hyperparameter values, improving classification performance. The effectiveness of the DSC-EDLMGWO approach is evaluated using a benchmark image database, with outcomes measured across various performance metrics. The experimental validation of the DSC-EDLMGWO approach portrayed a superior accuracy value of 98.38% and 98.17% under HAM10000 and ISIC datasets across other techniques. The limitations of the DSC-EDLMGWO approach comprise its reliance on a single dataset, which may not fully represent the diversity of real-world scenarios in skin cancer detection. Furthermore, the performance of the model might degrade when applied to unseen or highly variable data, such as images from diverse devices or environmental conditions. The computational complexity of the proposed approach could also restrict its applicability in real-time or resource-constrained environments. Future work can improve the model's generalization capability by testing it on a broader range of datasets and integrating data augmentation techniques. Moreover, optimizing the model for faster processing without sacrificing accuracy would increase its practical use. Exploring TL for enhanced model adaptation to new domains could also be a valuable direction for future research.

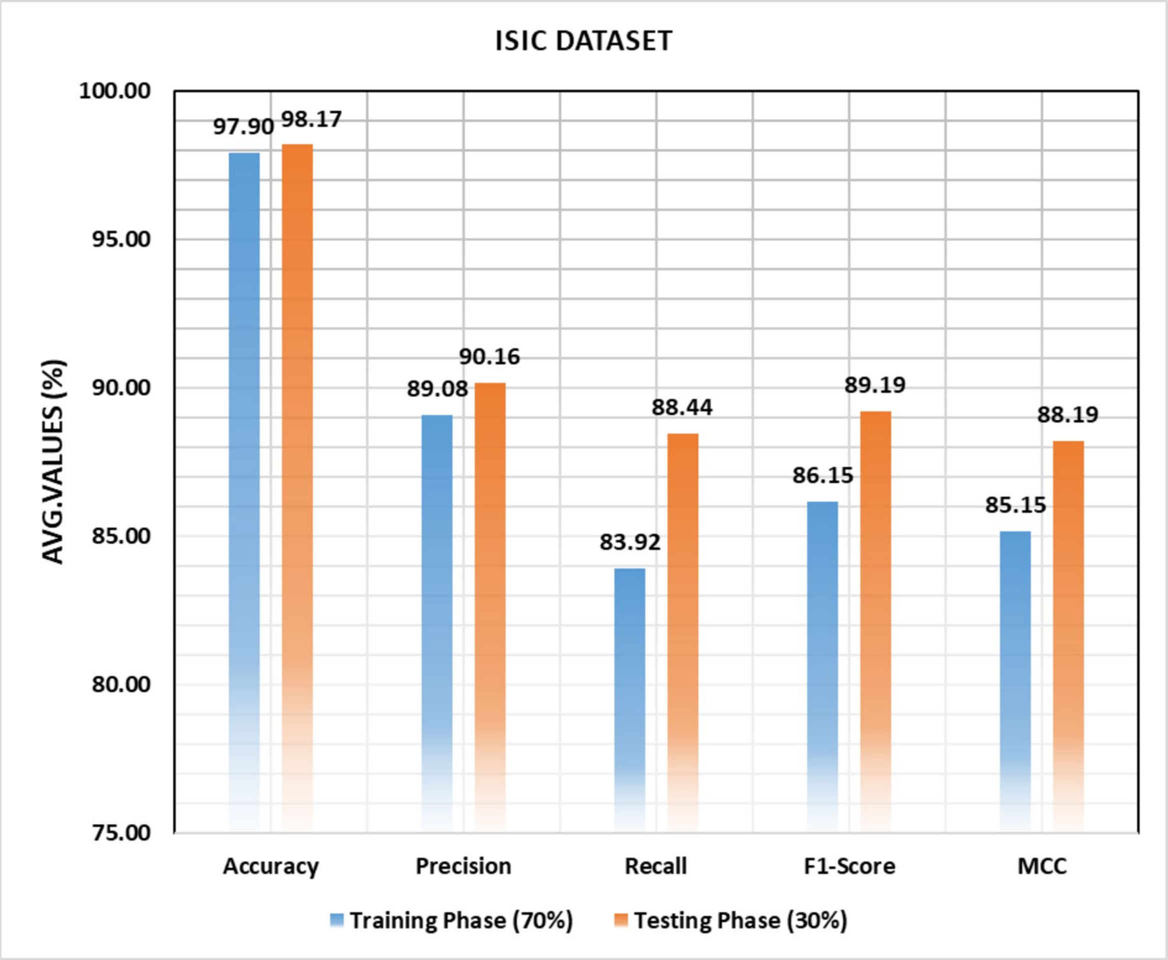

Fig. 12. Average of DSC-EDLMGWO model on ISIC database.

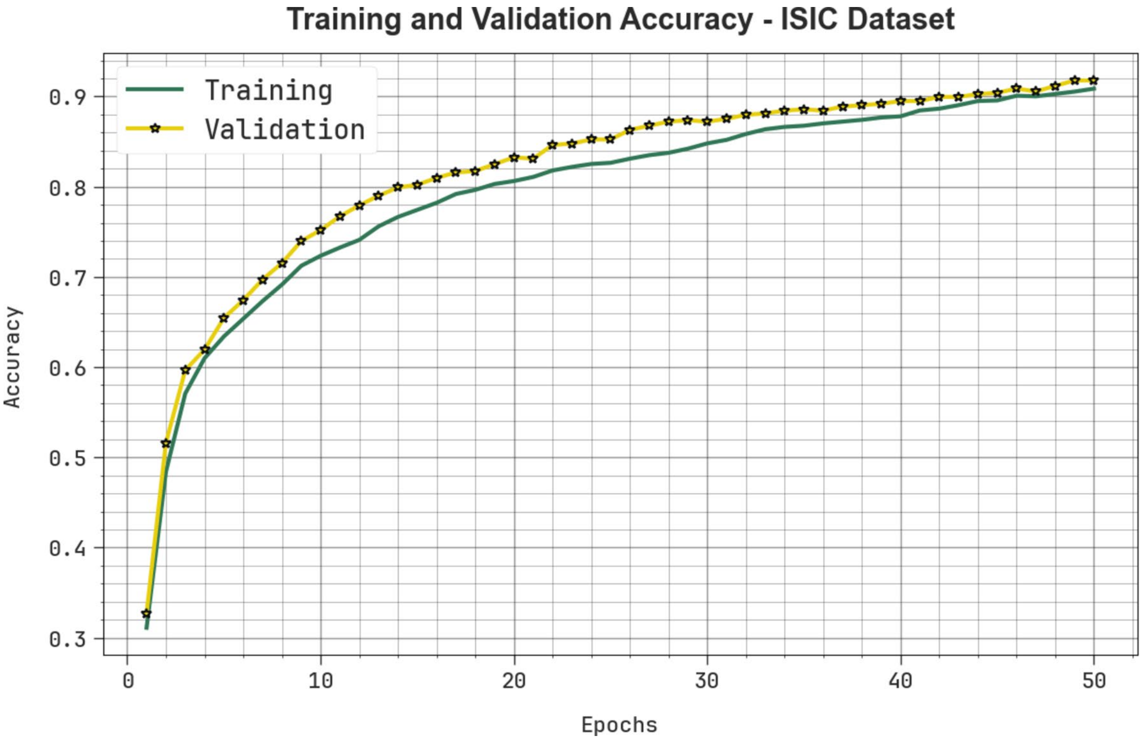

Fig. 13. $Accu_y$ graph of DSC-EDLMGWO model on ISIC database.

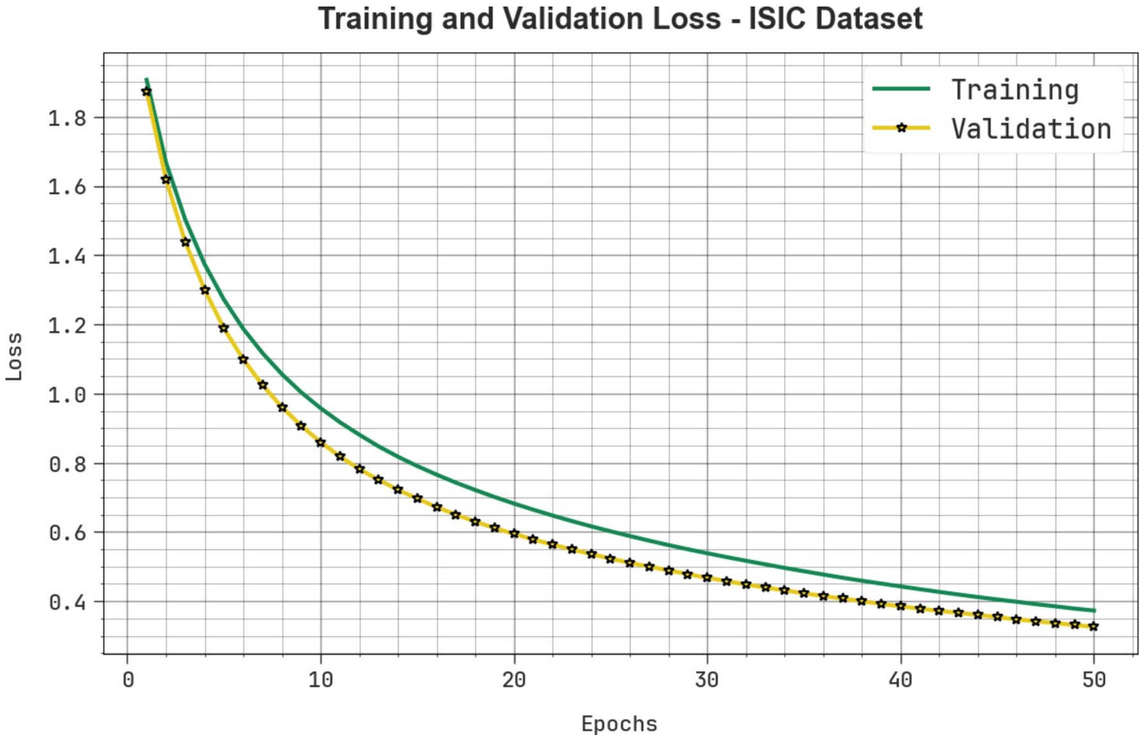

Fig. 14. Loss analysis of DSC-EDLMGWO technique on ISIC database.

ISIC Database				
Framework	$Accu_y$	$Prec_n$	$Reca_l$	$F1_{score}$
DSC-EDLMGWO	98.17	90.16	88.44	89.19
VGG19 Algorithm	80.17	85.63	82.86	84.33
MAFCNN-SCD	92.23	77.10	83.72	74.33
Ensemble CNN-EfficientNet	89.75	81.21	78.18	84.33
ResNet-152	84.15	85.05	83.14	84.55
Efficient-B7	84.87	74.98	83.62	88.85
DenseNet169 Model	89.44	87.91	85.89	79.55
SCC-DCNNTLM	91.93	88.26	81.06	75.47
DSCC-Net SMOTE Tomek	94.17	89.66	82.44	86.42

Table 7. Comparative analysis of the DSC-EDLMGWO model on the ISIC database[52–55].

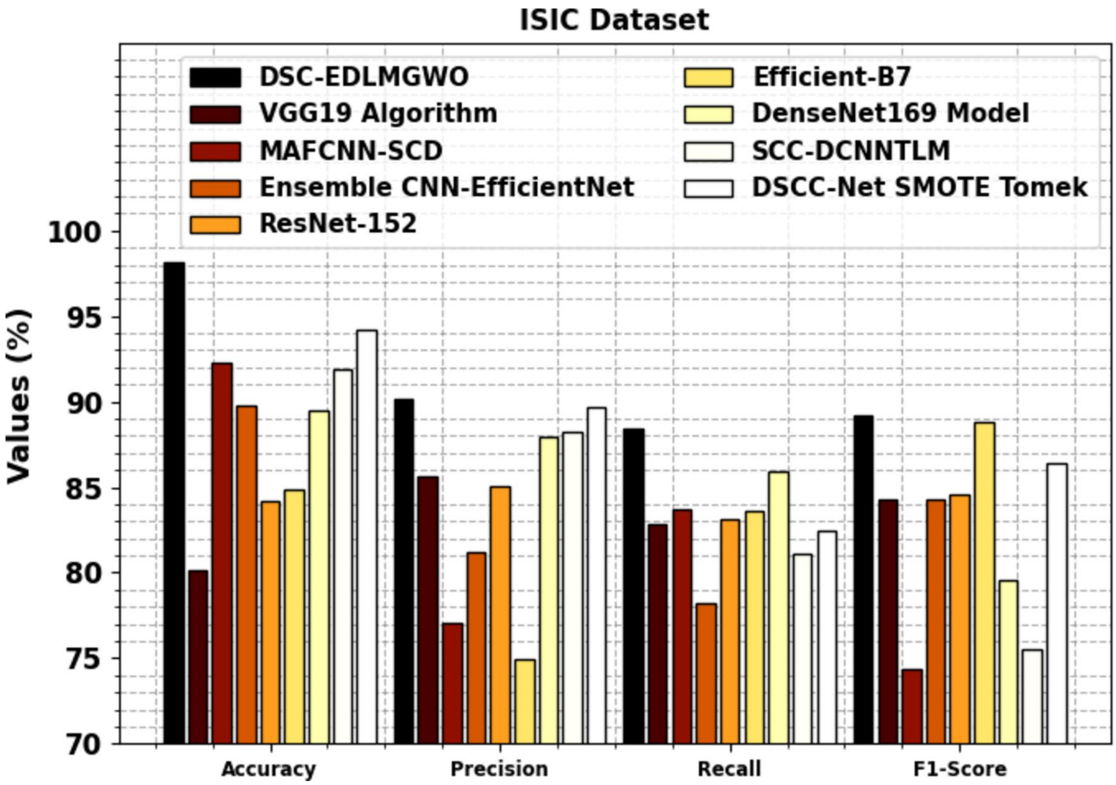

Fig. 15. Comparative analysis of the DSC-EDLMGWO model on the ISIC database.

ISIC Database	
Framework	**CT (sec)**
DSC-EDLMGWO	7.12
VGG19 Algorithm	12.64
MAFCNN-SCD	14.43
Ensemble CNN-EfficientNet	14.02
ResNet-152	14.51
Efficient-B7	10.96
DenseNet169 Model	12.34
SCC-DCNNTLM	11.71
DSCC-Net SMOTE Tomek	14.62

Table 8. CT evaluation of the DSC-EDLMGWO model on the ISIC dataset.

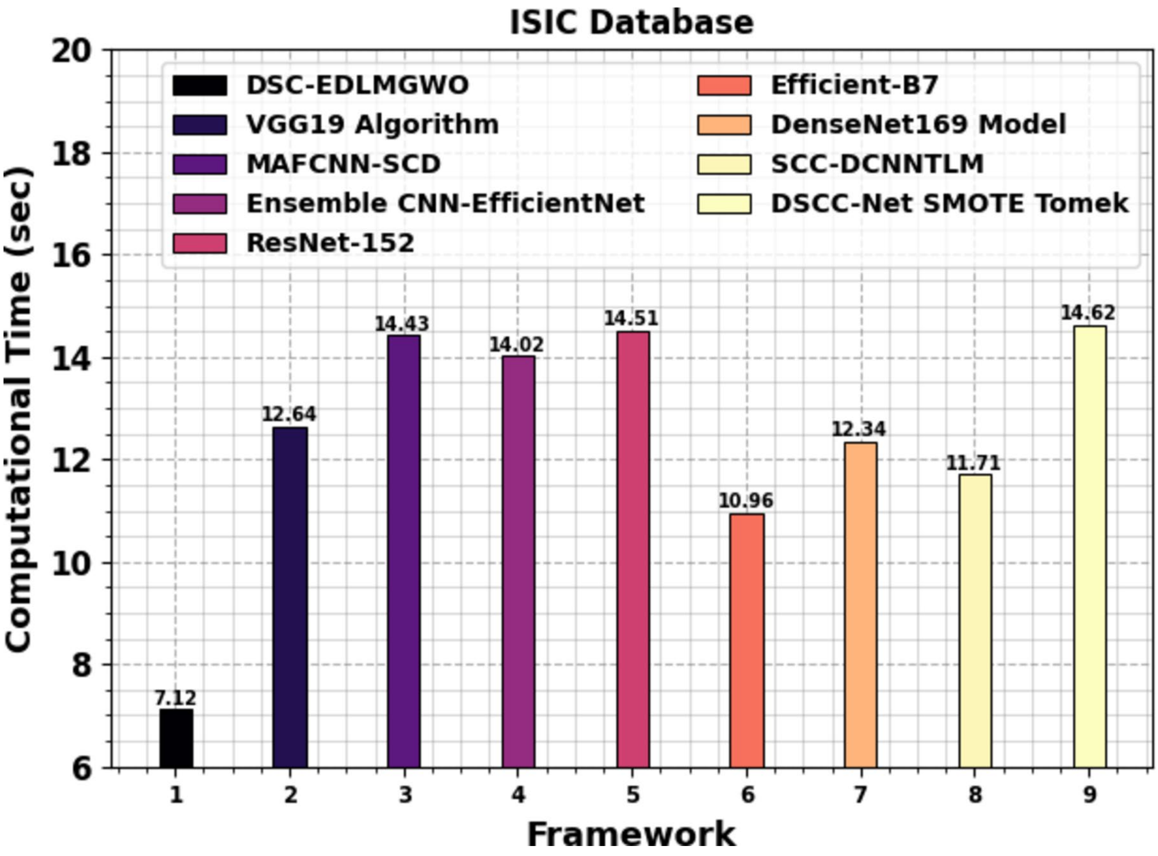

Fig. 16. CT evaluation of the DSC-EDLMGWO model on the ISIC dataset.

Data availability

The data that support the findings of this study are openly available in the Kaggle repository at https://www.kaggle.com/datasets/kmader/skin-cancer-mnist-ham10000, and https://www.kaggle.com/datasets/nodoubttome/skin-cancer9-classesisic reference number[26,27].

Received: 19 December 2024; Accepted: 26 February 2025

References

1. Adegun, A. & Viriri, S. Deep learning techniques for skin lesion analysis and melanoma cancer detection: A survey of the state-of-the-art. *Artif. Intell. Rev.* **54**, 811–841 (2021).
2. Kadampur, M. A. & Al Riyaee, S. Skin cancer detection: applying a deep learning based model driven architecture in the cloud for classifying dermal cell images. *Inf. Med. Unlocked*. **18**, 100282 (2020).
3. Jojoa Acosta, M. F., Tovar, C., Garcia-Zapirain, L. Y. & Percybrooks, M. B. Melanoma diagnosis using deep learning techniques on dermatoscopic images. *BMC Med. Imaging*. **21**, 1–11 (2021).

4. Rey-Barroso, L. et al. Optical technologies for the improvement of skin cancer diagnosis: A review. *Sensors* **21**, 252 (2021).
5. Al-Saqal, O. E., Hadied, Z. A. & Algamal, Z. Y. Modeling bladder cancer survival function based on neutrosophic inverse Gompertz distribution. *Int. J. Neutrosophic Sci. (IJNS)* **25**(1), 75–80 (2025).
6. Hasan, M. R., Fatemi, M. I., Khan, M. M., Kaur, M. & Zaguia, A. Comparative Analysis of Skin Cancer (Benign vs. Malignant) Detection Using Convolutional Neural Networks. J. Healthc. Eng. 2021, 5895156. (2021).
7. Kaur, R., Hosseini, H. G., Sinha, R. & Lindén, M. Melanoma classification using a novel deep convolutional neural network with dermoscopic images. *Sensors* **22**, 1134 (2022).
8. Algamal, Z. Y., Alobaidi, N. N., Hamad, A. A., Alanaz, M. M. & Mustafa, M. Y. Neutrosophic Beta-Lindley distribution: mathematical properties and modeling bladder Cancer data. *Int. J. Neutrosophic Sci.* **23** (2), 186–194 (2024).
9. Daghrir, J., Tlig, L., Bouchouicha, M. & Sayadi, M. September. Melanoma skin cancer detection using deep learning and classical machine learning techniques: A hybrid approach. In *2020 5th international conference on advanced technologies for signal and image processing (ATSIP)* (pp. 1–5). IEEE. (2020).
10. Selmi, A. & Issaouı, I. Enhancing skin Cancer diagnosis using cubic pythagorean fuzzy hypersoft set with salp swarm algorithm. *Int. J. Neutrosophic Sci.* **25**(1), 148–159 (2025).
11. Farea, E., Saleh, R. A., AbuAlkebash, H., Farea, A. A. & Al-antari, M. A. A hybrid deep learning skin cancer prediction framework. *Engineering Science and Technology, an International Journal*, *57*, p.101818. (2024).
12. Keerthana, D., Venugopal, V., Nath, M. K. & Mishra, M. Hybrid convolutional neural networks with SVM classifier for classification of skin cancer. *Biomedical Engineering Advances*, *5*, p.100069. (2023).
13. Saleh, N., Hassan, M. A. & Salaheldin, A. M. Skin cancer classification is based on an optimized convolutional neural network and multicriteria decision-making. *Scientific Reports*, *14*(1), p.17323. (2024).
14. Albawi, S., Arif, M. H. & Waleed, J. Skin cancer classification dermatologist-level based on deep learning model. *Acta Scientiarum Technol.* **45**, e61531–e61531 (2023).
15. Likhon, M. N. H. et al. SkinMultiNet: advancements in skin cancer prediction using deep learning with web interface. *Biomed. Mater. Devices* **2**, 1–17 (2024).
16. Singh, S. K., Abolghasemi, V. & Anisi, M. H. Fuzzy logic with deep learning for detection of skin cancer. *Applied Sciences*, *13*(15), p.8927. (2023).
17. Musthafa, M. M., TR, M. & Guluwadi, S. V, V.K. and Enhanced skin cancer diagnosis using optimized CNN architecture and checkpoints for automated dermatological lesion classification. *BMC Medical Imaging*, *24*(1), p.201. (2024).
18. Inthiyaz, S. et al. Skin disease detection using deep learning. *Advances in Engineering Software*, *175*, p.103361. (2023).
19. Huang, H., Wu, N., Liang, Y., Peng, X. & Shu, J. SLNL: a novel method for gene selection and phenotype classification. *Int. J. Intell. Syst.* **37** (9), 6283–6304 (2022).
20. Ozdemir, B. & Pacal, I. An innovative Deep learning framework for skin cancer detection employing ConvNeXtV2 and focal self-attention mechanisms. *Results in Engineering*, *25*, p.103692. (2025).
21. Wang, H. et al. Merge-and-Split Graph Convolutional Network for Skeleton-Based Interaction Recognition. *Cyborg and Bionic Systems*, *5*, p.0102. (2024).
22. Pacal, I. Investigating deep learning approaches for cervical cancer diagnosis: a focus on modern image-based models. *Eur. J. Gynaecol. Oncol.* **46**(1), 25–141 (2025).
23. Cui, Q., Ding, Z. & Chen, F. Hybrid Directed Hypergraph Learning and Forecasting of Skeleton-Based Human Poses. *Cyborg and Bionic Systems*, *5*, p.0093. (2024).
24. Bayram, B., Kunduracioglu, I., Ince, S. & Pacal, I. A systematic review of deep learning in MRI-based cerebral vascular occlusion-based brain diseases. *Neuroscience*. (2025).
25. Pacal, I., Alaftekin, M. & Zengul, F. D. Enhancing skin Cancer diagnosis using Swin transformer with hybrid shifted Window-Based Multi-head Self-attention and SwiGLU-Based MLP. *J. Imaging Inf. Med.* **37**, 1–19 (2024).
26. Khan, S. U. R., Asif, S., Zhao, M., Zou, W. & Li, Y. Optimize brain tumor multiclass classification with manta ray foraging and improved residual block techniques. *Multimedia Syst.* **31** (1), 1–27 (2025).
27. Bing, P. et al. A novel approach for denoising electrocardiogram signals to detect cardiovascular diseases using an efficient hybrid scheme. *Frontiers in Cardiovascular Medicine*, *11*, p.1277123. (2024).
28. Khan, M. A., Alam, S. & Ahmed, W. Enhanced skin Cancer diagnosis via deep convolutional neural networks with ensemble learning. *SN Comput. Sci.* **6** (2), 1–14 (2025).
29. Song, W. et al. Centerformer: a novel cluster center enhanced transformer for unconstrained dental plaque segmentation. *IEEE Trans. Multimedia* **26** (2024).
30. Das, A. & Mohanty, M. N. Design of stacked ensemble classifier for skin cancer detection. *Multimedia Tools and Applications*, pp.1–20. (2025).
31. Jia, Y., Chen, G. & Chi, H. Retinal fundus image super-resolution based on generative adversarial network guided with vascular structure prior. *Scientific Reports*, *14*(1), p.22786. (2024).
32. Ozdemir, B. & Pacal, I. A robust deep learning framework for multiclass skin cancer classification. *Scientific Reports*, *15*(1), p.4938. (2025).
33. Bilal, A. et al. Breast cancer diagnosis using support vector machine optimized by improved quantum inspired grey wolf optimization. *Scientific Reports*, *14*(1), p.10714. (2024).
34. Sainudeen, J. P. & Sathyalakshmi, S. Skin cancer classification using ensemble classification model with improved deep joint segmentation. *Int. J. Bioinform. Res. Appl.* **21** (1), 72–101 (2025).
35. Bilal, A. et al. BC-QNet: A quantum-infused ELM model for breast cancer diagnosis. *Computers in Biology and Medicine*, *175*, p.108483. (2024).
36. Akter, M. et al. *An Integrated Deep Learning Model for Skin Cancer Detection Using Hybrid Feature Fusion Technique*pp.1–15 (Biomedical Materials & Devices, 2025).
37. Bilal, A., Liu, X., Shafiq, M., Ahmed, Z. & Long, H. NIMEQ-SACNet: A novel self-attention precision medicine model for vision-threatening diabetic retinopathy using image data. *Computers in Biology and Medicine*, *171*, p.108099. (2024).
38. Vidhyalakshmi, A. M. & Kanchana, M. *Optimizing Skin Cancer Diagnosis: A Modified Ensemble Convolutional Neural Network for Classification* (Microscopy Research and Technique, 2025).
39. Wu, Z., Huang, R., Sun, W., He, B. & Wang, C. Clinical characteristics, treatment and outcome of subacute cutaneous lupus erythematosus induced by PD-1/PD-L1 inhibitors. *Arch. Dermatol. Res.* **316** (10), 1–7 (2024).
40. Chiu, T. M., Li, Y. C., Chi, I. C. & Tseng, M. H. AI-Driven Enhancement of Skin Cancer Diagnosis: A Two-Stage Voting Ensemble Approach Using Dermoscopic Data. *Cancers*, *17*(1), p.137. (2025).
41. Pacal, I. A novel Swin transformer approach utilizing residual multi-layer perceptron for diagnosing brain tumors in MRI images. *Int. J. Mach. Learn. Cybernet.* **15**, 1–19 (2024).
42. Reis, H. C. & Turk, V. DSCIMABNet: A novel multi-head attention depthwise separable CNN model for skin cancer detection. *Pattern Recognition*, *159*, p.111182. (2025).
43. Hosseinzadeh, M. et al. A model for skin cancer using combination of ensemble learning and deep learning. *Plos One*. **19** (5), e0301275 (2024).
44. Yu, C. Y., Lin, H. Y., Ouyang, Y. C. & Yu, T. W. Modulated AIHT image contrast enhancement algorithm based on contrast-limited adaptive histogram equalization. *Appl. Math. Inform. Sci.* **7**, 449–454 (2013).

45. Amudha, M. & Brindha, K. Rice leaf nutrient deficiency classification system using CAR-Capsule network. *IEEE Access.* **12**, 169518–169532 (2024).
46. Li, C., Chen, X., Zhang, L. & Wang, S. Determination of Coniferous Wood's Compressive Strength by SE-DenseNet Model Combined with Near-Infrared Spectroscopy. *Applied Sciences*, *13*(1), p.152. (2022).
47. Liu, Z., Zhao, A. R. & Liu, S. L. Prediction of Fading for Painted Cultural Relics Using the Optimized Gray Wolf Optimization-Long Short-Term Memory Model. *Applied Sciences*, *14*(21), p.9735. (2024).
48. Fares, N., Souaidia, C. & Thelaidjia, T. Extreme learning machine based on BDE feature selection to detect fault scenarios in grid-connected PV systems under MPPT mode. *Stud. Eng. Exact Sci.* **5** (2), e9473–e9473 (2024).
49. Majumdar, A. Blind denoising autoencoder. *IEEE Trans. Neural Networks Learn. Syst.* **30** (1), 312–317 (2018).
50. Awad, R., Budayan, C. & Gurgun, A. P. Construction and Demolition Waste Generation Prediction by Using Artificial Neural Networks and Metaheuristic Algorithms. *Buildings*, *14*(11), p.3695. (2024).
51. https://www.kaggle.com/datasets/kmader/skin-cancer-mnist-ham10000
52. Obayya, M. et al. A.E. and Henry gas solubility optimization algorithm based feature extraction in dermoscopic images analysis of skin cancer. *Cancers*, *15*(7), p.214. (2023).
53. Hoang, L., Lee, S. H., Lee, E. J. & Kwon, K. R. Multiclass skin lesion classification using a novel lightweight deep learning framework for smart healthcare. *Applied Sciences*, *12*(5), p.2677. (2022).
54. Zia Ur Rehman, M. et al. Classification of skin cancer lesions using explainable deep learning. *Sensors*, *22*(18), p.6915. (2022).
55. Abou Ali, M., Dornaika, F., Arganda-Carreras, I., Ali, H. & Karaouni, M. Naturalize revolution: unprecedented AI-Driven precision in skin Cancer classification using deep learning. *BioMedInformatics* **4** (1), 638–660 (2024).
56. https://www.kaggle.com/datasets/nodoubttome/skin-cancer9-classesisic

Author contributions

J. D. Dorathi Jayaseeli: Conceptualization, methodology development, experiment, formal analysis, investigation, writing. J Briskilal: Formal analysis, investigation, validation, visualization, writing. C. Fancy: Formal analysis, review and editing. V. Vaitheeshwaran : Methodology, investigation. R S M Lakshmi Patibandla: Review and editing.Anil Kumar Swain: Discussion, review and editing. Khasim Syed: Conceptualization, methodology development, investigation, supervision, review and editing.All authors have read and agreed to the published version of the manuscript.

Declarations

Competing interests

The authors declare no competing interests.

Ethics approval

This article contains no studies with human participants performed by any authors.

Informed consent

Informed consent was obtained from all subjects.

Consent to participate

Not applicable.

Additional information

Correspondence and requests for materials should be addressed to K.S.

Reprints and permissions information is available at www.nature.com/reprints.

Publisher's note Springer Nature remains neutral with regard to jurisdictional claims in published maps and institutional affiliations.